
CHAPTER 29, PART I

VIBRATION OF STRUCTURES INDUCED BY FLUID FLOW

R. D. Blevins

INTRODUCTION

Fluid around a structure can significantly alter the structure's vibrational characteristics. The presence of a quiescent fluid decreases the natural frequencies and increases the damping of the structure. A dense fluid couples the vibration of elastic structures which are adjacent to each other. Fluid flow can induce vibration. A turbulent fluid flow exerts random pressures on a structure, and these random pressures induce a random response. The structure can resonate with periodic components of the wake. If a structure is sufficiently flexible, the structural deformation under the fluid loading will in turn change the fluid force. The response can be unstable with very large structural vibrations—once the fluid velocity exceeds a critical threshold value.

Vibration induced by fluid flow can be classified by the nature of the fluid-structure interaction as shown in Fig. 29.1. Effects which are largely independent of viscosity include added mass and inertial coupling. Unsteady pressure on the surface of a structure, due to either variations in the free stream flow or turbulent fluctuations, induces a forced vibration response. Strong fluid-structure interaction phenomena result when the fluid force on a structure induces a significant response which in turn alters the fluid force. These phenomena are discussed in this section.

ADDED MASS AND INERTIAL COUPLING

If a body accelerates, decelerates, or vibrates in a fluid, then fluid is entrained by the body. This entrainment of fluid, called the *added mass* or *virtual mass effect*, occurs both in viscous and in inviscid, i.e., ideal, fluids. It is of practical importance when the fluid density is comparable to the density of the structure because then the added mass becomes a significant fraction of the total mass in dynamic motion.

Consider the rigid body shown in Fig. 29.2 which lies in a reservoir of incompressible inviscid irrotational fluid. The surface S defines the surface of the body. The body moves with velocity $U(t)$. From ideal flow theory, it can be shown that there exists a

INERTIAL COUPLING EFFECTS	UNSTEADY FLOW INDUCED VIBRATION	FLOW-STRUCTURE COUPLED VIBRATION
1. Added mass 2. Inertial coupling 3. Instability due to parallel flow	1. Turbulence induced vibration 2. Ocean wave induced vibration 3. Sonic fatigue	1. Vortex induced vibration 2. Galloping and flutter 3. Fluid elastic instability

FIGURE 29.1 A classification of flow-induced vibration.

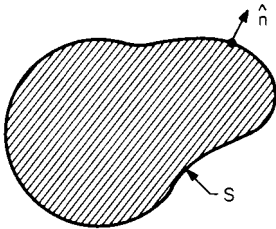


FIGURE 29.2 Fluid-filled region. Fluid density ρ .

velocity potential $\Phi(x, y, z, t)$ which is a function of the special coordinates and time, such that the velocity vector is the gradient of a potential function:

$$\mathbf{V} = \nabla\Phi \tag{29.1}$$

$\mathbf{V}(x, y, z, t)$ is the fluid velocity vector. The potential function Φ satisfies Laplace's equation:^{1,2}

$$\nabla^2\Phi = 0 \tag{29.2}$$

The boundary condition is that on the surface of the body; the normal component of velocity must equal the velocity of the body:

$$\frac{\partial\Phi}{\partial\mathbf{n}} = \mathbf{V} \cdot \mathbf{n} \quad \text{on the surface } S$$

where \mathbf{n} is the unit outward normal vector. The pressure in the fluid is given by the Bernoulli equation

$$p = -\rho \frac{\partial\Phi}{\partial t} - \frac{1}{2} \rho V^2$$

where ρ is the fluid density and V is the magnitude of \mathbf{V} . The force exerted by the fluid on the body is the integral of the fluid pressure over the surface.

$$\mathbf{F} = \int_S p \mathbf{n} \, dS$$

If the fluid is of infinite extent, then the solution of these equations is considerably simplified. The fluid force is¹

$$\mathbf{F} = -\rho \frac{\partial}{\partial t} \int_S \Phi \mathbf{n} \, dS \tag{29.3}$$

and flow potential can be expressed as $\phi = U(t)\phi(x', y', z')$, where $x', y',$ and z' are coordinates that are fixed to the body and U is the flow velocity relative to the body. Substituting this potential in Eq. (29.3) yields the following force:

$$F = -m \frac{\partial U}{\partial t} \quad (29.4)$$

where the added mass m is

$$m = \rho \int_S \phi \frac{\partial \phi}{\partial n} dS \quad (29.5)$$

The added mass force Eq. (29.3) is zero for U and Φ independent of time, i.e., for steady translation. This is the D'Alembert paradox for an ideal inviscid fluid flow; the fluid force is not zero for steady translation in a viscous fluid.

As an example of added mass calculation, the potential for flow over a cylinder of radius a is

$$\phi = U \frac{r^2 + a^2}{r} \cos \theta$$

where r = radial coordinate
 θ = angular coordinate
 U = flow velocity

The added mass per unit length is found from Eq. (29.5). The result is

$$m = \rho \pi a^2$$

where a is the cylinder radius. This added fluid mass is equal to the mass of fluid displaced by the cylinder.

In general, there will be an added mass tensor to represent the added mass for acceleration in each of the three coordinate directions:

$$m_{ij} = \rho \int_S \phi_j \frac{\partial \phi_i}{\partial n} dS$$

and an added mass tensor for rotation about the three coordinate axes. ϕ_i is the potential associated with flow in the i direction. Note that the added mass tensor is symmetric, i.e., $m_{ij} = m_{ji}$, but if the body is not symmetric, there is coupling between motions in the various coordinate directions.¹ For example, if a body is not symmetric about the X axis, acceleration in the X direction generally induces added mass force in the Y direction and a moment as well.

Since the added mass acts in phase with acceleration [Eq. (29.3)], the net effect of added mass is to increase the effective mass of the body and to decrease the natural frequencies. In general, added mass is only important to mechanical structures in dense fluids such as water. In gases, such as air, the added mass is ordinarily negligible except for very lightweight structures. Figure 29.3 gives added mass for various sections and bodies in large unrestricted reservoirs. Additional tables of added mass are given in Refs. 3 and 4.

If two structures are in close proximity, then the added mass will be a function of the spacing between the structures and inertial coupling will be introduced between the bodies. For example, consider a cylindrical rod centered in a fluid-filled annulus bounded by a cylindrical cavity shown in Fig. 29.4. The radius of the rod is a and the


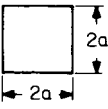
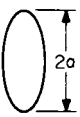
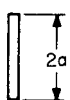

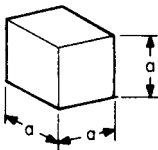
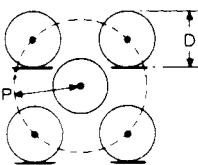
GEOMETRY		ADDED MASS
1. CIRCULAR CYLINDER OF RADIUS a .		$\rho\pi a^2 b$
2. SQUARE SECTION OF SIDE $2a$.		$1.51\rho\pi a^2 b$
3. ELLIPTICAL SECTION WITH MAJOR RADIUS a .		$\rho\pi a^2 b$
4. FLAT PLATE OF HEIGHT $2a$.		$\rho\pi a^2 b$
5. SPHERE OF RADIUS a .		$\frac{2}{3}\rho\pi a^3$
6. CUBE OF SIDE a .		$0.7\rho a^3$
7. CYLINDER IN ARRAY OF FIXED CYLINDERS		$\frac{\rho\pi D^2 b}{4} \left[\frac{(D_e/D)^2 + 1}{(D_e/D)^2 - 1} \right]$ WHERE $D_e/D = (1 + \frac{1}{2}P/D)P/D$

FIGURE 29.3 Added mass for lateral acceleration.³ The acceleration is left to right. b is the span for two-dimensional sections.

radius of the outer cylinder is b . The fluid forces exerted on the rod and outer cylinder because of their relative acceleration are⁵

$$\begin{aligned}
 F_1 &= -m\ddot{x}_1 + (M_1 + m)\ddot{x}_2 \\
 F_2 &= (m + M_1)\ddot{x}_1 - (m + M_1 + M_2)\ddot{x}_2
 \end{aligned}
 \tag{29.6}$$

where x_1, x_2 = displacement of inner rod and outer cylinder
 F_1, F_2 = force on inner rod and outer cylinder
 $m = \rho\pi a^2(b^2 + a^2)/(b^2 - a^2)$, added mass of inner rod
 $M_1 = \rho\pi a^2$
 $M_2 = \rho\pi b^2$

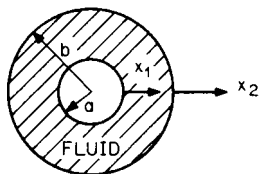


FIGURE 29.4 A rod in a fluid-filled annulus.

These forces include not only added mass but also inertial coupling between the motion of the two structures. [These equations also apply for a sphere contained within a spherical cavity but here $m = (M_1/2)(b^3 - 2a^3)/(b^3 - a^3)$, $M_1 = \frac{2}{3}\rho\pi a^3$, and $M_2 = \frac{4}{3}\rho\pi b^3$.] Coupling is introduced through the fluid annulus. The coupling increases with the density of the fluid

and decreases with increasing gap. If the cylinder and the rod are elastic, motion of either structure tends to set both structures into motion.

For example, consider an array of heat exchanger tubes contained within a shell. Water fills the shell and surrounds the tubes. If the tubes are widely spaced (more than about two diameters between centers), then the tubes are largely uncoupled and the effect of added mass is simply to reduce the tube natural frequencies by the addition of fluid equal to the displaced volume of the tubes. However, if the tubes are closely spaced, then motion of one tube sets adjacent tubes and the shell into motion. Fluid-coupled modes of vibration will result in the tubes and the shell moving in fixed modal patterns as shown in Fig. 29.5. In Refs. 6 and 7, analysis is given for inertial coupling of a cylinder contained eccentrically within a cylindrical cavity, rows of cylinders, and arrays of cylinders.



FIGURE 29.5 Coupled modes of vibration of a bank of tubes in a dense fluid.⁶

Added mass and inertial coupling occur in elastic and rigid bodies, but the added complexity of elasticity and the three-dimensional motions make a closed-form solution impossible for most elastic bodies. In the case of quasi-two-dimensional structures (such as long span tubes or rods), the axial variation in the motion occurs relatively slowly over the span, and two-dimensional results for sections are applicable. Concentric cylindrical shells coupled by a fluid annulus are important in the design of nuclear reactor containment vessels. Approximate solutions are required for both the vessels and the fluid. Reviews of the analysis of fluid coupled concentric vessels are given in Refs. 8 and 9.

Finite element numerical solutions, developed for an irrotational fluid, have been incorporated in the NASTRAN and other computer programs to permit solution for added mass and inertial coupling. These programs solve the fluid and structural problems and then couple the results through interaction forces¹⁰ (see Chap. 28, Part II).

WAVE-INDUCED VIBRATION OF STRUCTURES

Waves induce vibration of structures, such as marine pipelines, oil terminals, tanks, and ships, by placing oscillatory pressure on the surface of the structure. These forces are often well-represented by the inviscid flow solution for many large structures such as ships and oil storage tanks. For most smaller structures, viscous effects influence the fluid force and the fluid forces are determined experimentally.

Consider an ocean wave approaching the vertical cylindrical structure as shown in Fig. 29.6. The wave is propagating in the X direction. Using small-amplitude (lin-

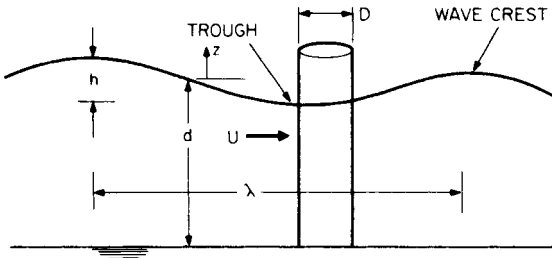


FIGURE 29.6 A circular cylindrical structure exposed to ocean waves.

ear) inviscid wave theory, the wave is characterized by the wave height h (vertical distance between trough and crest), its angular frequency ω , and the associated wavelength λ (horizontal distance between crests), and d is the depth of the water. The wave potential Φ satisfies Laplace’s equation [Eq. (29.2)] and a free-surface boundary condition.¹¹ The associated horizontal component of wave velocity varies with depth $-z$ from the free surface and oscillates at frequency ω :

$$U(t, z) = \frac{h\omega}{2} \frac{\cosh [2\pi(z + d)/\lambda]}{\sinh (2\pi d/\lambda)} \cos \left(\frac{2\pi x}{\lambda} - \omega t \right) \quad (29.7)$$

This component of wave velocity induces substantial fluid forces on structures, such as pilings and pipelines, which are oriented perpendicular to the direction of wave propagation.

The forces which the wave exerts on the cylinder in the direction of wave propagation (i.e., in line with U) can be considered the sum of three components: (1) a buoyancy force associated with the pressure gradient in the laterally accelerating fluid [Eq. (29.7)], (2) an added mass force associated with fluid entrained during relative acceleration between the fluid and the cylinder [Eq. (29.4)], and (3) a force due to fluid dynamic drag associated with the relative velocity between the wave and the cylinder. The first two force components can be determined from inviscid fluid analysis as discussed previously. The drag component of force, however, is associated with fluid viscosity.

Thus, the in-line fluid force per unit length of cylinder due to an unsteady flow is expressed as the sum of the three fluid force components:

$$F = \rho A \dot{U} + C_I \rho A (\ddot{U} - \ddot{x}) + \frac{1}{2} \rho |U - \dot{x}| (U - \dot{x}) D C_D \quad (29.8)$$

where x = lateral position of structure in direction of wave propagation
 A = cross-sectional area = $\frac{1}{4}\pi D^2$ of cylinder having diameter D
 C_I = added mass coefficient, which has theoretical value of 1.0 for circular cylinder
 C_D = drag coefficient

This is the generalized form of the Morison equation, widely used to compute the wave forces on slender cylindrical ocean structures such as pipelines and piers.

If \dot{x} and \ddot{x} are set equal to zero in Eq. (29.8), the incline force per unit length on a stationary cylinder in an oscillating flow is obtained:

$$F(\dot{x} = \ddot{x} = 0) = C_m \rho A \dot{U} + \frac{1}{2} \rho |U| U D C_D \quad (29.9)$$

Because of the absolute sign in the term $|U| U$, the force contains not only components at the wave frequency but also components associated with the drag at harmonics of the wave frequency. The resultant time-history of in-line force due to a harmonically oscillating flow has an irregular form that repeats once every wave period.

If the flow oscillates with zero mean flow, $U = U_0 \cos \omega t$ as in Eq. (29.7), then the maximum fluid force per unit length on a stationary cylinder is

$$F_{\max} = \begin{cases} \rho A C_m \omega U_0 & \text{if } \frac{U_0}{\omega D} < \frac{C_m A}{C_D D^2} \\ \frac{1}{2} \rho U_0^2 D C_D + \frac{(\rho A C_m U_0 \omega)^2}{2\pi U_0^2 D C_D} & \text{if } \frac{U_0}{\omega D} > \frac{C_m A}{C_D D^2} \end{cases} \quad (29.10)$$

If the cylinder is large (such as for a storage tank) with diameter D greater than the ocean wave height h and if the wavelength of the ocean wave is comparable to the diameter, then U_0 is small compared to ωD and the maximum force is given by the first alternative in Eq. (29.10). The drag force is negligible compared to the inertial forces for large cylinders. As a result, the ocean wave forces on large cylinders can be calculated using inviscid, i.e., potential flow, methods which are discussed in Refs. 11 and 12.

For the Reynolds number ranges typical of most offshore structures, measurements show that the inertial coefficient $C_m = 1 + C_I$ for cylindrical structures generally falls in the range between 1.5 and 2.0. $C_m = 1.8$ is a typical value. C_m decreases for very large diameter cylinders owing to the tendency of waves to diffract about large cylinders (Refs. 13 and 14). Similarly, measurements show that the drag coefficient falls between 0.6 and 1.0 for circular cylinders; $C_D = 0.8$ is a typical value.

Wave forces on elastic ocean structures induce structural motion. Since the wave force is nonlinear [Eq. (29.8)] and involves structural motion, no exact solution exists. One approach is to integrate the equations of motion directly by applying Eq. (29.8) at each spanwise point on a structure and then numerically integrate the time-history of deflection using a predictor-corrector or recursive relationship to account for the nonlinear term. A simpler approach is to assume that the structural deformation does not influence the fluid force and apply Eq. (29.9) as a static load. This static approximation is valid as long as the fundamental natural frequency of the structure is well above the wave frequency and the first three or four harmonics of the wave frequency. However, many marine structures are not sufficiently stiff to satisfy this condition.

One generally valid simplification for dynamic analysis of relatively flexible structures is to consider that the wave velocity is much less than the structural velocity so

that $|U - \dot{x}| \approx |U|$. With this approximation, application of Eq. (29.8) to a single degree-of-freedom model for a structure gives the following linear equation of motion:

$$(m + \rho AC_I)\ddot{x} + (2\zeta\omega_N + \frac{1}{2}\rho |U| DC_D)\dot{x} + kx = \rho AC_m \dot{U} + \frac{1}{2}\rho |U| U DC_D \quad (29.11)$$

where m = structural mass per unit length
 k = stiffness
 ζ = structural damping

This equation is solved by expanding both $x(t)$ and $U(t)$ in a Fourier series and matching the coefficients.

The fluid forces contribute added mass and fluid damping to the left-hand side as well as forcing terms to the right-hand side. This equation may be simplified further by retaining only the first (constant) term in the series expansion for $|U|$ in the fluid damping term so that the equation becomes a classical forced oscillator with constant coefficient.¹²

Flexible structures will resonate with the wave if the structural natural period equals the wave period or a harmonic of the wave period. Since the wave frequencies of importance are ordinarily less than 0.2 Hz (wave period generally greater than one cycle per 5 sec), such a resonance occurs only for exceptionally flexible structures such as deep-water oil production risers and offshore terminals. The amplitude of structural response at resonance is a balance between the wave force and the structural stiffness times the damping. Since the wave force diminishes with increased structural motion [Eq. (29.8)], the resultant displacements are necessarily self-limiting. In other words, the response which would be predicted by applying Eq. (29.9) dynamically is overly pessimistic because the wave force contributes mass and damping to the structure as well as excitation as can be seen in Eq. (29.11).

The above discussion considers only fluid forces which act in line with the direction of wave propagation. These in-line forces produce an in-line response. However, substantial transverse vibrations also occur for ocean flows around circular cylinders. These vibrations are associated with periodic vortex shedding, which is discussed below. The models discussed in the following section for steady flow are applicable to vortex shedding in oscillatory flows provided that the wave period exceeds the period of shedding, based on the maximum oscillatory velocity so that it is possible to fit one or more shedding cycles into the wave cycle.^{13,14}

VORTEX-INDUCED VIBRATION

Many structures of practical importance such as buildings, pipelines, and cables are not streamlined but rather have abrupt contours that can cause a fluid flow over the structure to separate from the aft contours of the structure. Such structures are called *bluff bodies*. For a bluff body in uniform cross flow, the wake behind the body is not regular but contains distinct vortices of the pattern shown in Fig. 29.7 at a Reynolds number $Re = UD/\nu$ greater than about 50, where D is the width perpendicular to the flow and ν is the kinematic viscosity. The vortices are shed alternately from each side of the body in a regular manner and give rise to an alternating force on the body. Experimental studies have shown that the frequency, in hertz, of the alternating lift force is expressed as^{16,17}

$$f_s = \frac{SU}{D} \quad (29.12)$$

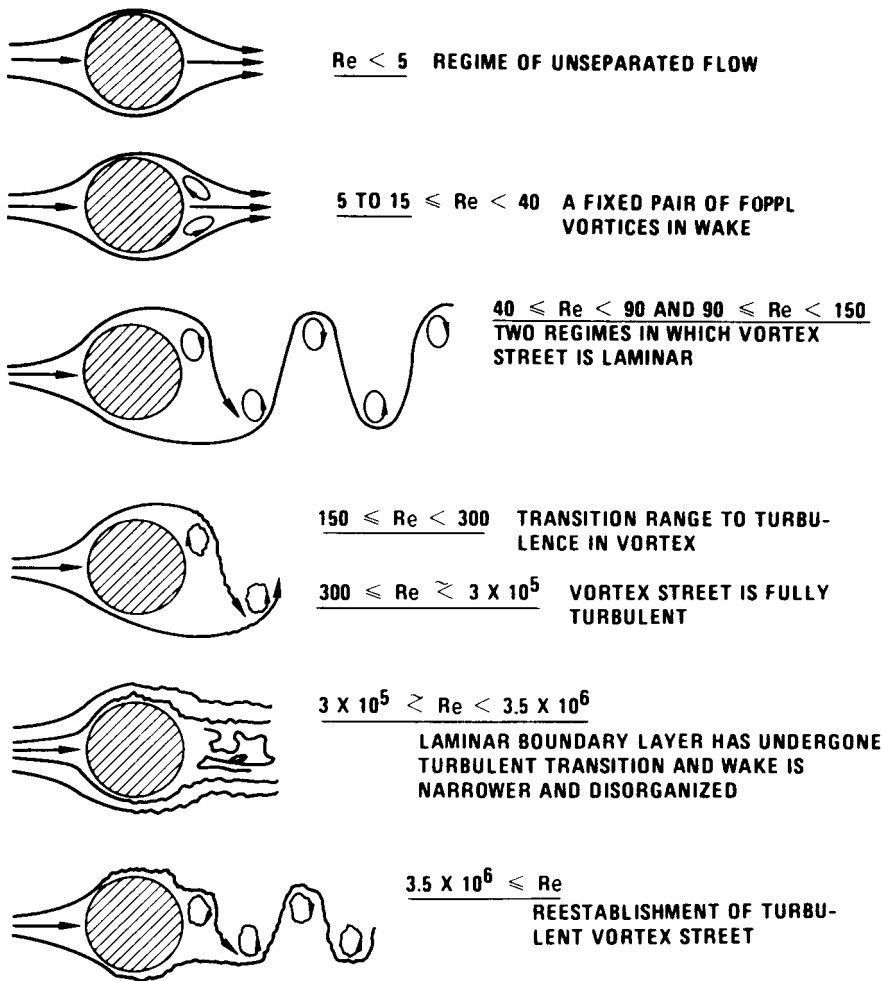


FIGURE 29.7 Regimes of fluid flow across circular cylinders.¹⁵

The dimensionless constant S called the *Strouhal number* generally falls in the range $0.25 \geq S \geq 0.14$ for circular cylinders, square cylinders, and most bluff sections. The value of S increases slightly as the Reynolds number increases; a value of $S = 0.2$ is typical for circular cylinders.

The oscillating lift force imposed on a single circular cylinder of length L and diameter D , in a uniform cross flow of velocity U , due to vortex shedding is given by

$$F = \frac{1}{2} \rho U^2 C_L D L \sin(2\pi f_s t) \quad (29.13)$$

where the lift coefficient C_L is a function of Reynolds number and cylinder motion. The experimental measurements of C_L show considerable scatter with typical values ranging from 0.1 to 1.0. The scatter is in part due to the fact that the alternating vor-

forces are not generally correlated on the entire cylinder length L . The spanwise correlation length l_c of vortex shedding over a stationary circular cylinder¹⁷ is approximately three to seven diameters for $10^3 < Re < 2 \times 10^5$. In order to account for the effect of the spanwise correlation on the net force on the cylinder of length L , a factor J called the *joint acceptance* has been introduced on the right-hand side of Eq. (29.13). Two limiting cases exist for the joint acceptance.

$$J = \begin{cases} \left(\frac{l_c}{L}\right)^{1/2} & \text{if } l_c \ll L \\ 1 & \text{if fully correlated} \end{cases}$$

Thus, if a cylinder is much longer than three to seven diameters, the lack of spanwise correlation reduces the net vortex lift force [Eq. (29.13)] on the cylinder.

Cylinder vibration at or near the vortex shedding frequency organizes the wake and changes the fluid force on the cylinder. Vibration of a cylinder in a fluid flow can:^{12,17,18}

1. Increase the strength of the shed vortices.
2. Increase the spanwise correlation of the vortex shedding.
3. Cause the vortex shedding frequency shift from the natural shedding frequency [Eq. (29.12)] to the frequency of cylinder oscillation. This is called *synchronization* or *lock-in*.
4. Increase the mean drag on the cylinder. Mean drag can triple for one diameter amplitude cylinder vibration.
5. Alter the phase sequence and pattern of vortices in the wake. Figure 29.8 shows the patterns of vortices in the wake of a transversely vibrating cylinder, where f_s = natural shedding frequency [Eq. (29.12)], f = forced vibration frequency, and A_y = vibration amplitude transverse to flow.

As the flow velocity is increased or decreased so that the shedding frequency f_s approaches the natural frequency f_n of an elastically mounted cylinder so that

$$f_n \approx f_s = \frac{SU}{D} \quad \text{so} \quad \frac{U}{f_n D} \approx \frac{U}{f_s D} = \frac{1}{S} \approx 5$$

the vortex shedding frequency suddenly locks onto the structure natural frequency. The resultant vibrations occur at or nearly at the natural frequency of the structure and vortices in the near wake input energy to the cylinder. Large amplitude vortex-induced structural vibration can result.

The vortex-induced vibrations of a spring-mounted cylinder in a flow are shown as a function of velocity in Fig. 29.9 for two levels of damping. The horizontal scale gives flow velocity nondimensionalized (i.e., divided by the cylinder diameter D times the cylinder natural frequency f), both of which are held fixed as velocity U increases. The lower part of the figure shows the measured response cylinder single amplitude A_y vibration response as a function of flow velocity. The maximum cylinder amplitude occurs at the resonance condition $U / (fD) \sim 5.5$. The upper part of the figure shows the vortex shedding frequency. The shedding frequency increases with velocity as predicted by Eq. (29.8) until it equals the cylinder natural frequency at $U/fD = 5$ and large amplitude cylinder vibrations begin. The shedding frequency

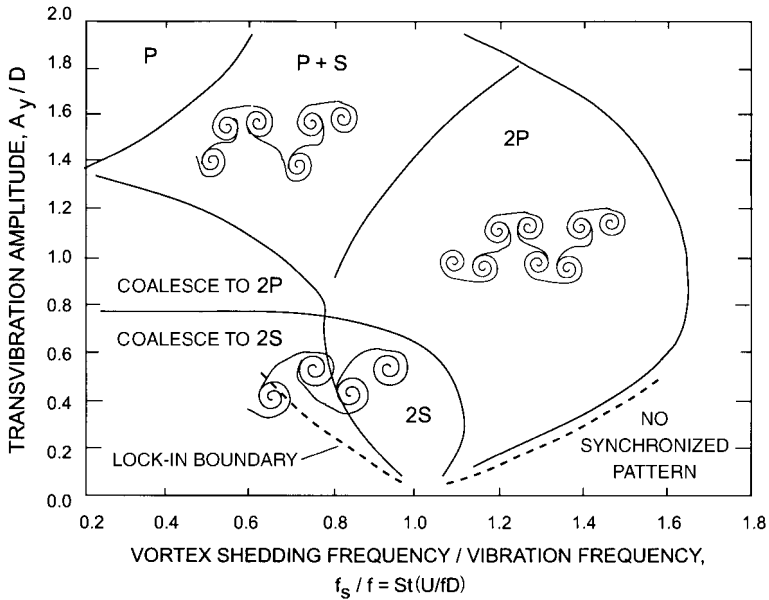


FIGURE 29.8 Patterns of vortices shed in the wake of a transversely oscillating cylinder in a cross flow.

is entrained by the cylinder natural frequency. Entrainment persists until velocity is increased to $U/fD = 6.5$ at which point lock-in is broken and the shedding frequency abruptly returns to its natural value. In general, the larger the structural response to vortex shedding, the larger the range of lock-in.

Both the amplitude of the structural response and the velocity range over which lock-in persists are functions of the dimensionless reduced damping parameter δ_r :

$$\delta_r = \frac{2m(2\pi\zeta)}{\rho D^2}$$

where m = mass per unit length of cylinder, including added mass
 ζ = damping factor for vibration in mode of interest, ordinarily measured in still fluid
 ρ = fluid density
 D = cylinder diameter

The lower δ_r , the greater the amplitude of the structural response and the greater the range of flow velocities over which lock-in occurs (see Ref. 19 and Fig. 29.8). For lightly damped structures in dense fluids (such as marine pipelines), δ_r is on the order of 1 and lock-in can persist over a 40 percent variation in velocity above and below that which produces resonance.

Within the synchronization band, substantial resonance vibration often occurs. Peak-to-peak vibration amplitudes of up to three diameters have been observed in water flows over cables and tubing. The vibrations are predominantly transverse to

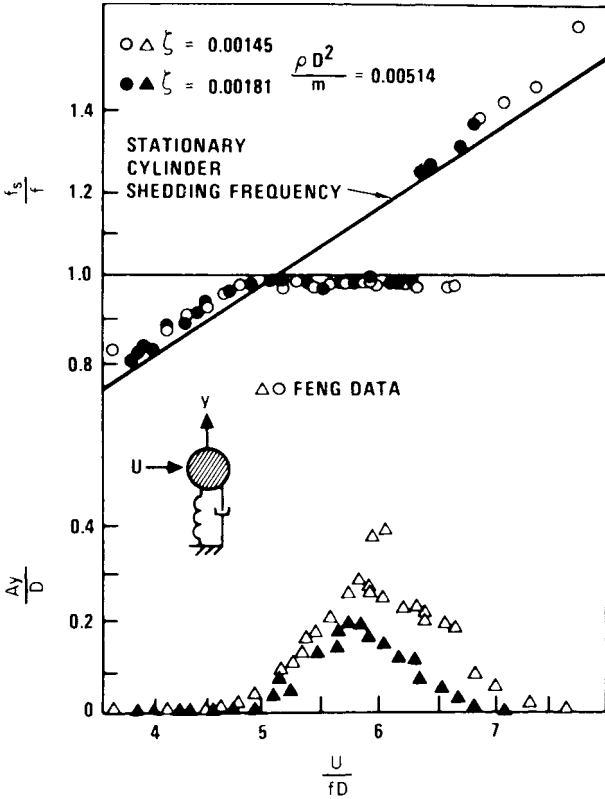


FIGURE 29.9 Response of a spring-supported cylinder to vortex-induced vibration.²⁰

the flow and are self-limiting.¹² Lesser amplitude vibrations have also been observed in the drag direction at twice the vortex shedding frequency and at subharmonic frequencies of the vortex shedding frequency, i.e., at one-fourth, one-third, or one-half of the flow velocity required for synchronization,²¹ $f_s = f_n$.

If a uniform elastic cylinder is subjected to a crossflow uniformly over its span, then the oscillating vortex-induced lift force is given by Eq. (29.13). At lock-in, the vortex shedding frequency equals the natural frequency of the n th vibration mode $f_s = f_n$, and the amplitude of the cylinder response is

$$\frac{A_y}{D} = \frac{C_L J}{4\pi S^2 \delta_v} \tag{29.14}$$

where the maximum amplitude vibrations along the span are $y(t) = A_y \sin(2\pi f_n t)$. This equation is conservative if $C_L = J = 1$. However, Eq. (29.14) gives overly conservative predictions with $C_L = J = 1$ owing to the tendency of the actual lift coefficient to decrease at amplitudes in excess of 0.5 diameters and the lack of perfect spanwise correlation at large amplitudes. Semiempirical correlations are given in Refs. 12, 22, and 23. One of these correlations is¹²

$$\frac{A_y}{D} = \frac{0.07\gamma}{(\delta_r + 1.9)S^2} \left(0.3 + \frac{0.72}{(\delta_r + 1.9)S} \right)^{1/2} \tag{29.15}$$

The mode shape parameter γ falls between 1.0 and 1.4. For a translating rigid rod ($\phi = 1$), $\gamma = 1$, for a cable or pipeline with a sinusoidal mode shape, $\gamma = 1.15$ and for a cantilever mode shape, $\gamma = 1.4$ and A_y is tip amplitude.

Equation (29.15) correctly predicts the self-limiting behavior of the resonance vibrations. Setting damping to zero, $\delta_r = 0$, it follows that $A_y/D \approx 1.5$, which is a typical vibration level for lightly damped marine cables in a current. See Fig. 29.10. Large amplitude vibrations also are associated with increased steady drag on the structure. Drag coefficients of up to 3.5 have been measured on resonantly vibrating marine cables as opposed to the typical value of 1.0 for a stationary cylinder.²⁴

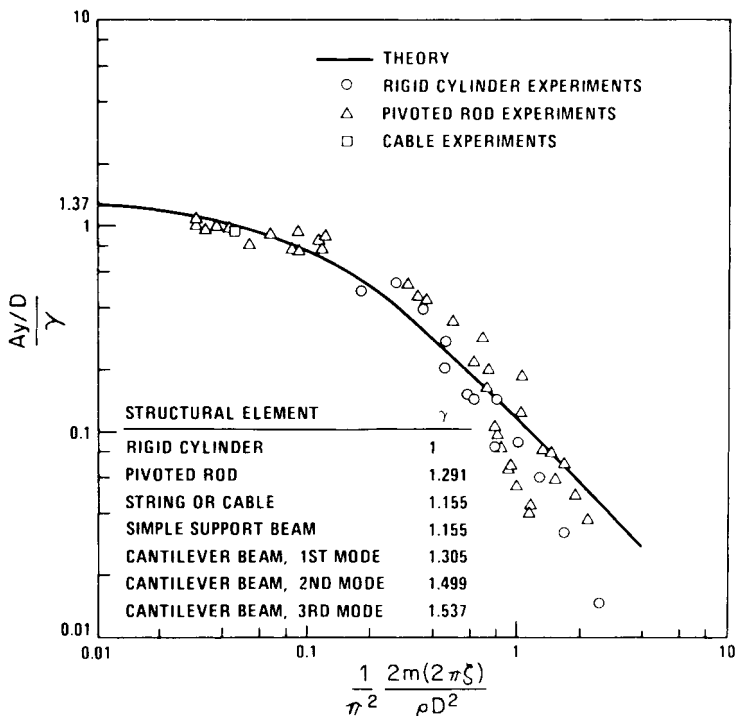


FIGURE 29.10 Maximum amplitude of vortex-induced vibration as a function of damping.¹²

A number of fairings, strakes, and ribbons have been attached to the exterior of circular cylindrical structures to reduce vortex-induced vibrations as shown in Fig. 29.11. These devices act by disrupting the near wake and disturbing the correlation between the vortex shedding and vibration. They do, however, increase the steady drag from that which is measured on a stationary structure. Reviews of vortex suppression devices are given in Refs. 25 and 26.

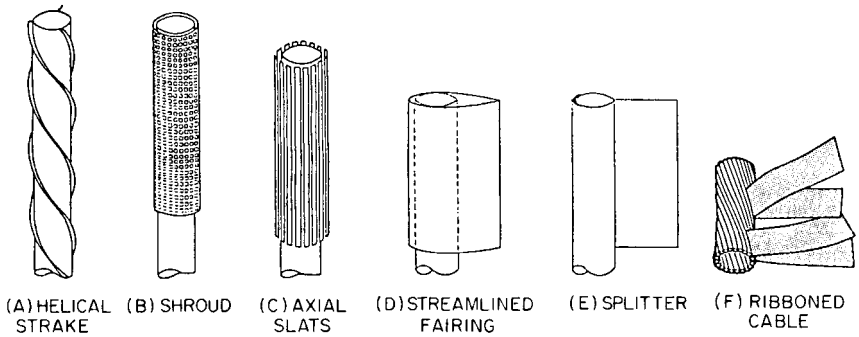


FIGURE 29.11 Methods of reducing vortex-induced vibration.

FLUID ELASTIC INSTABILITY

Fluid flow across an array of elastic tubes can induce a dynamic instability, resulting in very large amplitude tube vibrations once the critical cross-flow velocity is exceeded. This is a relatively common occurrence in tube and shell heat exchangers. Once the critical cross-flow velocity is exceeded, vibration amplitude increases very rapidly with cross-flow velocity V , usually as V^n where $n = 4$ or more, compared with an exponent in the range $1.5 < n < 2.5$ below the instability threshold. This can be seen in Fig. 29.12, which shows the response of an array of metallic tubes to water flow. The initial hump is attributed to vortex shedding. The cross-flow velocity is defined as velocity perpendicular to the tube axis at the minimum gap between tubes. Once the critical velocity is exceeded, the very large amplitude vibrations usually lead to failures of the heat exchanger tubes.

Often the large amplitude vibrations vary in time; the amplitudes grow and fall about a mean value in pseudorandom fashion. Generally the tubes do not move independently but instead move in somewhat synchronized orbits with neighboring tubes. This orbital behavior has been observed in tests in both air and water with orbits ranging from near circles to nearly straight lines. See Fig. 29.13.

As the tubes whirl in orbital motion, they extract energy from the fluid (Refs. 12, 28, and 29). Below the onset of instability, energy which is extracted is less than the energy which is expended in damping. Above the critical velocity, the energy extracted from the flow by the tube motion exceeds the energy expended in damping, so the vibrations increase in amplitude. Restricting the motion or introducing frequency differences between one or more tubes often increases the critical velocity for onset of instability. Such increases in critical velocity are generally no greater than about 40 percent unless additional support is given to all tubes exposed to high velocity flow. Often the onset of instability is more gradual in a bank of tubes having tube-to-tube frequency differences than in a bank with identical tubes. Only a relatively small percentage of the tube will become unstable at one time. Flexible long-span tubes in areas of high flow velocity (such as at inlets) are most susceptible to the instability.

At cross-flow velocities beyond those which produce an onset of instability, damaging vibrations are encountered. The tube vibration amplitudes are limited by clashing with other tubes, by impacting with the tube supports, and by yielding of the tubes. Sustained operation in the unstable vibration regime ordinarily results in tube

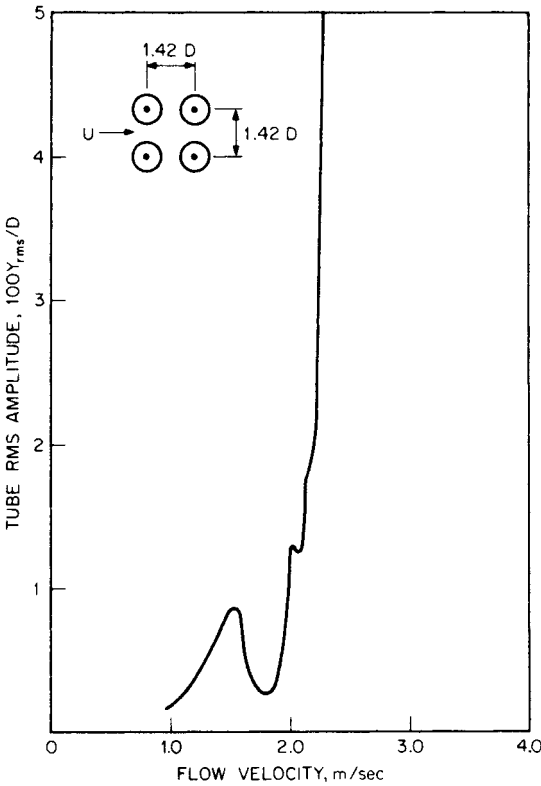


FIGURE 29.12 Typical amplitude of vibration of a tube array in cross flow.²⁷

failure due to wear or propagation of cracks in the tubes. Fluid elastic instability is second only to corrosion as a cause of heat exchanger failure.

A displacement model for the fluid elastic forces is given in Ref. 12 which correctly predicts the observed onset of instability for most cases in air and gases. Results are less satisfactory in water or when the motion of some of the tubes is restricted. More complex models take into account velocity-induced forces as well as the displacement-induced forces.^{29,30} These theories give somewhat better agreement with data over limited ranges, but none are entirely suitable for a design tool.

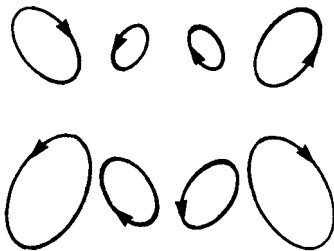


FIGURE 29.13 Tube vibration patterns for fluid elastic instability.²⁸

The most viable, practical procedure for predicting the onset of instability of closely spaced arrays of tubes to cross flow is to use the theoretical form given by the displacement mechanism but

with parameters obtained by fitting experimental data. The onset of instability is predicted as^{12,22,23,31}

$$\frac{V_{\text{crit}}}{f_n D} = C \left[\frac{m_t(2\pi\zeta)}{\rho D^2} \right]^a \quad (29.16)$$

where V_{crit} = uniform cross flow averaged over minimum gap between tubes (If the velocity is nonuniform, then either the maximum can be used or a modal weighted average can be employed.)

f_n = fundamental natural frequency of tubing (Ordinarily the fundamental mode is most susceptible to instability.)

ζ = damping factor of fundamental mode (Typically ζ falls in the range between 0.01 and 0.03 for tubes with some intermediate supports. For rolled-in or welded-in tubes with no intermediate supports, ζ can be as low as 0.001.)

m_t = mass per unit length of tube including added mass and internal mass of fluid

ρ = fluid density

Fitting Eq. (29.16) to the available 174 data points for onset of instability³¹ shown in Fig. 29.14 leads to the mean and lower-bound coefficients for the parameter C and the exponent a given in Table 29.1. The coefficient corresponding to the mean fit to the experimental data is C_{mean} ; $C_{90\%}$ is the lower bound fit to the data such that 90% of the data are above the curve.

Most of the data used in this correlation come from tube arrays with center-to-center spacing of between 1.25 and 2.0 diameters and with various array geometries. There is insufficient statistical evidence to determine if certain patterns are more or less susceptible to instability than others. Instability has been observed for both straight and curved tubes, tube rows, and tube arrays in a wide variety of tube patterns.

The most common means of increasing the resistance of an array of tubes to instability is to add intermediate supports to increase the natural frequency of the tubes. Details of the tube support (particularly the gap between the tube and the support) influence the resultant vibration. In general, smaller gaps tend to result in lower tube-support impact velocities and hence in lower tube wear.^{32,33}

INTERNAL FLOW IN PIPES

Internal flow through a pipe decreases the natural frequency of the pipe. Sufficiently high internal velocity will induce buckling in a pipe supported at both ends since the momentum of fluid turning through a small angle of pipe deflection is greater than the stiffness of the pipe. If the pipe is restrained at only one end, the pipe will become unstable at high velocities like an unrestrained garden hose.

The equation of motion for a straight pipe conveying steady fluid flow is^{34,35}

$$EI \frac{\partial^4 Y}{\partial x^4} + \rho A v^2 \frac{\partial^2 Y}{\partial x^2} + 2\rho A v \frac{\partial^2 Y}{\partial x \partial t} + M \frac{\partial^2 Y}{\partial t^2} = 0 \quad (29.17)$$

where E and I are the modulus and moment of inertia of the pipe which conveys fluid of density ρ through the internal area A of the pipe at a steady velocity v ; $Y(x, t)$ is the lateral deflection of the pipe which has total mass per unit length M .

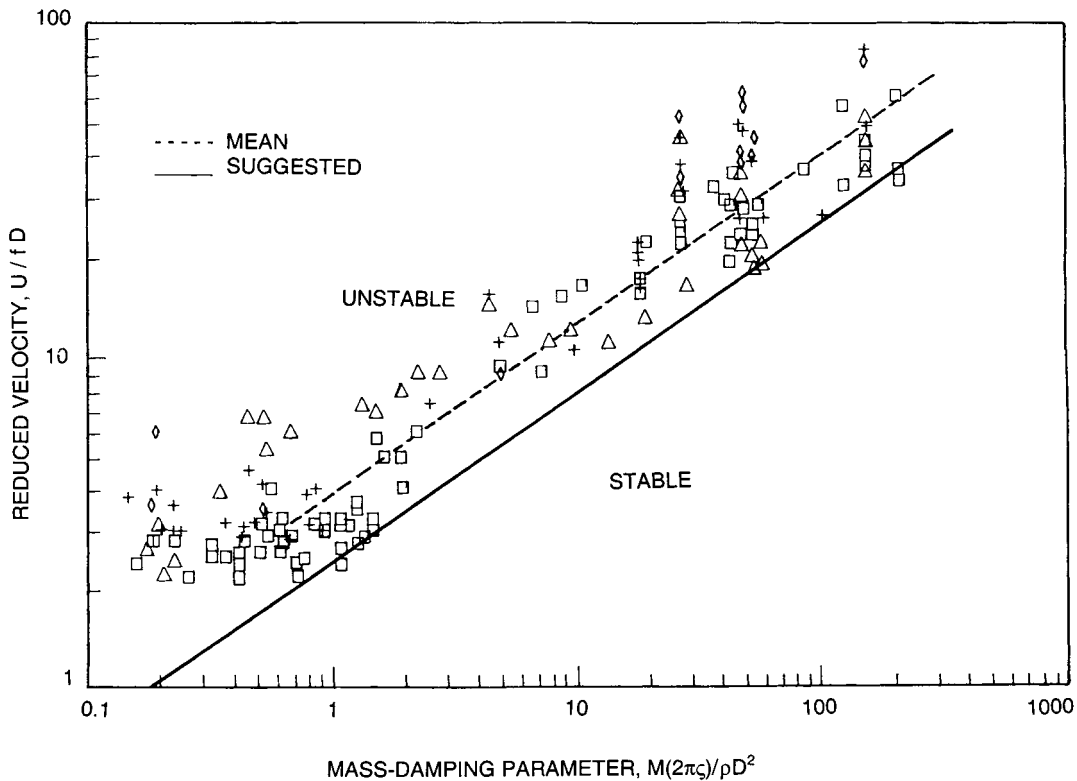


FIGURE 29.14 Velocity for onset of instability of tube arrays in cross flow as a function of the damping parameter.²²

TABLE 29.1 Coefficients in Eq. (29.16) for Onset of Instability of Tube Arrays³¹

	$m_i(2\pi\zeta)/\rho D^2 < 0.7$	$m_i(2\pi\zeta)/\rho D^2 > 0.7$
C_{mean}	3.9	4.0
$C_{90\%}$	2.7	2.4
a	0.21	0.5
rms error in fitted data for V_{crit} , %	24.5	32.5

The first and last terms in Eq. (29.17) are the usual stiffness and mass terms. The middle terms are associated with fluid forces imposed on the pipe by the internal fluid as the pipe deflects slightly from its equilibrium position.

Although Eq. (29.17) is a linear partial differential equation with constant coefficients, its solution is difficult owing to the mixed derivative term (third term from the left). One technique used to solve the equation is to expand the solution in terms of the mode shapes of vibration which are obtained for zero flow, $v = 0$.

$$Y(x, t) = \sum_i a_i y_i(x) \sin \omega t \quad (29.18)$$

where $y_i(x)$ are the mode shapes for zero flow that satisfy Eq. (29.17) and the boundary conditions on the ends of the pipe span. Equation (29.18) is substituted into Eq. (29.23), and the derivatives of $y_i(x)$ are expressed in terms of the orthogonal set $y_i(x)$

$$y_i'(x) = \sum_i b_i y_i(x)$$

Like terms in the series are equated.

For a uniform pipe with pinned ends, the result can be expressed as a decrease in natural frequency due to flow.¹²

$$\frac{f}{f_1} = \left[1 - \left(\frac{v}{v_c} \right)^2 \right]^{1/2} \quad (29.19)$$

where f = fundamental natural frequency
 f_1 = fundamental natural frequency in absence of flow
 v_c = critical flow velocity

The critical flow velocity can be expressed as

$$v_c = \frac{\pi}{L} \left[\frac{EI}{\rho A} \right]^{1/2} \quad (29.20)$$

where L is the span of the pipe. As the flow velocity approaches v_c , the fundamental natural frequency f_1 decreases to zero. The pipe span spontaneously buckles at $v = v_c$.

The buckling velocity is a function of the boundary conditions on the ends of the pipe, and there can be vibration; these solutions for various boundary conditions are generally scaled by the velocity v_c [Eq. (29.20)]. In general, only exceptionally thin-walled flexible tubes with very high velocity flows, such as rocket motor feed lines and penstocks, are prone to vibration induced by internal flow. External parallel flow can also induce an analogous instability. (See the review given in Ref. 35.) For a tube subjected to both internal and parallel external flow of the same magnitude, the velocity for the onset of instability is

$$v_c = \frac{\pi}{L} \left[\frac{EI}{\rho A_i + \rho A_e} \right]^{1/2} \quad (29.21)$$

where $A_i = \pi D_i^2/4$ and $A_e = \pi D_e^2/4$ are the cross-sectional areas associated with the tube inside and outside diameters D_i and D_e , respectively.

Oscillatory flow in pipes can also cause vibration. Oscillations of fluids in pipes can be caused by reciprocating pumps and acoustic oscillations produced by flow through valves and obstructions. Internal flow imposes net fluid force on pipe at bends and changes in area. For example, the fluid force acting on a 90° bend in a pipe is the sum of pressure and momentum components:

$$F_{\text{bend}} = [(p - p_a) + \rho U^2] A \mathbf{i} - [(p - p_a) + \rho U^2] A \mathbf{j} \quad (29.22)$$

Here p is the internal pressure in the pipe, p_a is the pressure in the atmosphere surrounding the pipe, and U is the internal velocity in the pipe. The vectors \mathbf{i} and \mathbf{j} are unit vectors in the direction of the incoming and outgoing fluid, respectively.

If the pressure and velocity in the pipe oscillates, then the fluid force on the bend will oscillate, causing pipe vibration in response to the internal flow. This problem is most prevalent in unsupported bends in pipe that are adjacent to pumps and valves. Two direct solutions are to (1) support pipe bends and changes in area so that fluid forces are reacted to ground and (2) reduce fluid oscillations in pipe by avoiding large pressure drops through valves and installation of oscillation-absorbing devices on pump inlet and discharge.

REFERENCES

1. Newman, J. N.: "Marine Hydrodynamics," The MIT Press, Cambridge, Mass., 1977.
2. Lamb, H.: "Hydrodynamics," Dover Publications, New York, 1945. Reprint of 6th ed., 1932.
3. Blevins, R. D.: "Formulas for Natural Frequency and Mode Shape," Kreiger, Malabar, Florida, 1984. Reprint of 1979 edition.
4. Milne-Thompson, L. L.: "Theoretical Hydrodynamics," 5th ed., Macmillan, New York, 1968.
5. Fritz, R. J.: *J. Eng. Industry*, **94**:167 (1972).
6. Chen, S-S: *J. Eng. Industry*, **97**:1212 (1975).
7. Chen, S-S: *Nucl. Eng. Des.*, **35**:399 (1975).
8. Brown, S. J.: *J. Pressure Vessel Tech.*, **104**:2 (1982).
9. Au-Yang, M. K.: *J. Vibration, Acoustics*, **108**:339 (1986).
10. Zienkiewicz, O. C.: "The Finite Element Method," 3d ed., McGraw-Hill Book Company, Inc., New York, 1977.
11. Ippen, A. T. (ed.): "Estuary and Coastline Hydrodynamics," McGraw-Hill Book Company, Inc., New York, 1966.
12. Blevins, R. D.: "Flow-Induced Vibration," 2d ed., Kreiger, Malibar, Fla., 1994.
13. Sarpkaya, T., and M. Isaacson: "Mechanics of Wave Forces on Offshore Structures," Van Nostrand Reinhold, New York, 1981.
14. Obasaju, E. D., P. W. Bearman, and J. M. R. Graham: *J. Fluid Mech.*, **196**:467 (1988).

15. Lienard, J. H.: "Synopsis of Lift, Drag and Vortex Frequency Data for Rigid Circular Cylinder," Washington State University, College of Engineering, Research Division Bulletin 300, 1966.
16. Roshko, A.: "On the Development of Turbulent Wakes from Vortex Streets," *National Advisory Committee for Aeronautics Report NACA TN-2913*, 1953.
17. Sarpkaya, T.: *J. Appl. Mech.*, **46**, 241 (1979).
18. Williamson, C. H. K., and A. Roshko: *J. Fluids and Structures*, **2**:355 (1988).
19. Scruton, C.: "On the Wind Excited Oscillations of Stacks, Towers and Masts," *National Physical Laboratory Symposium on Wind Effects on Buildings and Structures, Paper 16*, 790, 1963.
20. Feng, C. C.: "The Measurement of Vortex-Induced Effects in Flow Past Stationary and Oscillating Circular and D-Section Cylinder," M.A.Sc. thesis, University of British Columbia, 1968.
21. Durgin, W. W., P. A. March, and P. J. Lefebvre: *J. Fluids Eng.*, **102**:183 (1980).
22. ASME Boiler and Pressure Vessel Code, Section III, Division 1, Appendix N-1300, 1998.
23. Au-Yang, M. K., T. M. Mulcahy, and R. D. Blevins: *Pressure Vessel Technology*, **113**:257 (1991).
24. Vandiver, J. K.: "Drag Coefficients of Long Flexible Cylinders," *1983 Offshore Technology Conference, Paper 4490*, 1983, p. 405.
25. Zdravkovich, M. M.: *J. Wind Eng., Industrial Aerodynamics*, **7**:145 (1981).
26. Wong, H. Y., and A. Kokkalis: *J. Wind Eng. Industrial Aerodynamics*, **10**:21 (1982).
27. Chen, S-S, J. A. Jendrzejczyk, and W. H. Lin: "Experiments on Fluid Elastic Instability in a Tube Bank Subject to Liquid Cross Flow," *Argonne National Laboratory Report ANL-CT-44*, July 1978.
28. Connors, H. J.: "Fluid Elastic Vibration of Tube Arrays Excited by Cross Flow," Paper presented at the Symposium on Flow Induced Vibration in Heat Exchangers, ASME Winter Annual Meeting, December 1970.
29. Paidoussis, M. P., and S. J. Price: *J. Fluid Mech.*, **187**:45 (1988).
30. American Society of Mechanical Engineers. "Flow-Induced Vibrations—1994," PVP-273, New York, 1994.
31. Blevins, R. D.: *J. Sound & Vibration*, **97**:641 (1984).
32. Blevins, R. D.: *J. Eng. Materials Tech.*, **107**:61 (1985).
33. Cha, J. H.: *J. Pressure Vessel Tech.*, **109**:265 (1987).
34. Housner, G. W.: *J. Appl. Mech.*, **19**:205 (1952).
35. Paidoussis, M. P., and P. Besancon: *J. Sound & Vibration*, **76**:361 (1981).

CHAPTER 29, PART II

VIBRATION OF STRUCTURES INDUCED BY WIND

Alan G. Davenport
Milos Novak

INTRODUCTION

Vibration of significant magnitude may be induced by wind in a wide variety of structures including buildings, television and cooling towers, chimneys, bridges, transmission lines, and radio telescopes. No structure exposed to wind seems entirely immune from such excitation. The material presented here describes several mechanisms causing these oscillations and suggests a few simpler approaches that may be taken in design to reduce vibration of structures induced by wind. There is an extensive literature¹⁻⁵ giving a more detailed treatment of the subject matter.

FORMS OF AERODYNAMIC EXCITATION

The types of structure referred to above are generally unstreamlined in shape. Such shapes are termed “bluff bodies” in contrast to streamlined “aeronautical” shapes discussed in Chap. 29, Part III. The distinguishing feature is that when the air flows around such a bluff body, a significant wake forms downstream, as illustrated in Fig. 29.15. The wake is separated from the outside flow region by a shear layer. With a sharp-edged body (such as a building or structural member) as in Fig. 29.15, this shear layer emanates from the corner. With oval bodies such as the cylinder in Fig. 29.15, the shear layer commences at a so-called *boundary layer* on the upstream surface at points *A* and *B* (the separation points) and becomes a free shear layer. The exact position of these separation points depends on a wide variety of factors, such as the roughness of the cylinder, the turbulence in the flow, and the Reynolds number $R = VD/\nu$, where V = flow velocity, D = diameter of the body, and ν = kinematic viscosity.

The flow illustrated in Fig. 29.15 represents the time-average picture which would

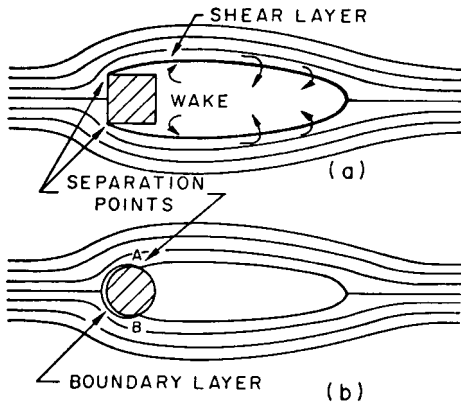


FIGURE 29.15 Wake formation past bluff bodies: (a) sharp-edged body; (b) circular cylinder.

be obtained by averaging the movements of the fluid particles over a time interval that is long compared with the “transit time” D/V . The instantaneous picture of the flow may be quite different, as indicated in Fig. 29.16, for two reasons.

First, if the flow is the wind, it is under almost all practical circumstances strongly turbulent; the oncoming flow will be varying continuously in direction and speed in an irregular manner. These fluctuating motions will range over a wide range of frequencies and scales (i.e., eddy sizes).

Second, the wake also will take on a fluctuating character. Here, however, the size of the dominant eddies (vortices) will be of a similar size to the body. The vortices tend to start off their career by curling up at the separation point and then are carried off downstream. Sometimes these eddies are fairly regular in character and are shed alternately from either side; if made visible by smoke or other means, they can be seen to form a more or less regular stepping-stone pattern until they are broken up by the turbulence or dissipate themselves. In a strongly turbulent flow, the regularity is disrupted.

The flow characteristics of the oncoming flow and the wake are the direct causes of the forces on the bodies responsible for their oscillation. The forms of the resulting oscillation are as follows.

1. Turbulence-induced oscillations. Certain types of oscillation of structures can be attributed almost exclusively to turbulence in the oncoming flow. In the wind these

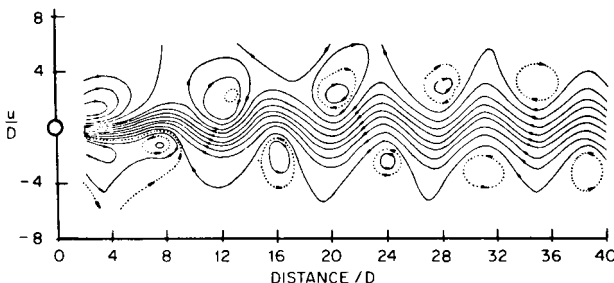


FIGURE 29.16 Vortex street past circular cylinder ($R = 56$). (After Kowasznay, Proc. Roy. Soc. London, 198, 1949.)

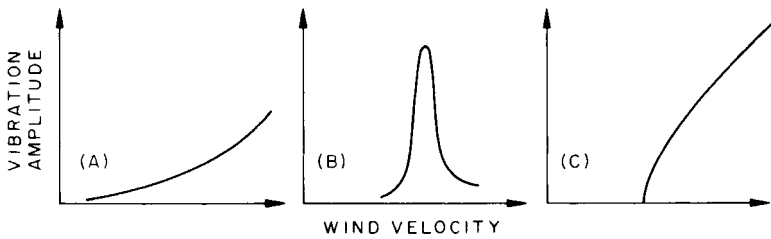


FIGURE 29.17 Main types of wind-induced oscillations: (A) vibration due to turbulence; (B) vibration due to vortex shedding; (C) aerodynamic instability.

may be described as “gust-induced oscillations” (or turbulence-induced, oscillations). The gusts may cause longitudinal, transverse, or torsional oscillations of the structure, which increase with wind velocity (Fig. 29.17).

2. Wake-induced oscillations. In other instances, the fluctuations in the wake may be the predominant agency. Since these fluctuations are generally characterized by alternating flow, first around one side of the body, then around the other, the most significant pressure fluctuations act on the sides of the body in the wake behind the separation point (the so-called *after body*); they act mainly laterally or torsionally and to a much lesser extent longitudinally. The resultant motion is known as *vortex-induced oscillation*. Oscillation in the direction perpendicular to that of the wind is the most important type. It often features a pronounced resonance peak (Fig. 29.17B).

While these distinctions between gust-induced and wake-induced forces are helpful, they often strongly interact; the presence of free-stream turbulence, for example, may significantly modify the wake.

3. Buffeting by the wake of an upstream structure. A further type of excitation is that induced by the wake of an upstream structure (Fig. 29.18). Such an arrangement of structures produces several effects. The turbulent wake containing strong vortices shed from the upstream structure can buffet the downstream structure. In addition, if the oncoming wind is very turbulent, it can cause the wake of the upstream structure to veer, subjecting the downstream structure successively to the free flow and the wake flow. This frequently occurs with chimneys in line, as well as with tall buildings.

4. Galloping and flutter mechanisms. The final mechanism for excitation is associated with the movements of the structure itself. As the structure moves relative to the flow in response to the forces acting, it changes the flow regime surrounding it. In so doing, the pressures change, and these changes are coupled with the motion. A pressure change coupled to the velocity (either linearly or nonlinearly) may be termed an *aerodynamic damping* term. It may be either positive or negative. If positive, it adds to the mechanical damping and leads to higher effective damping and a reduced tendency to vibrate; if negative, it can lead to instability and large amplitudes of movement. This type of excitation occurs with a wide variety of rectangular building shapes as well as bridge cross sections and common structural shapes such as angles and I sections.

In other instances, the coupling may be with either the displacement or acceleration, in which case they are described as either aerodynamic stiffness or mass terms, the effect of which is to modify the mass or stiffness terms in the equations of motion. Such modification can lead to changes in the apparent frequency of the structure. If the aerodynamic stiffness is negative, it can lead to a reduction in the effective stiffness of the structure and eventually to a form of instability known as

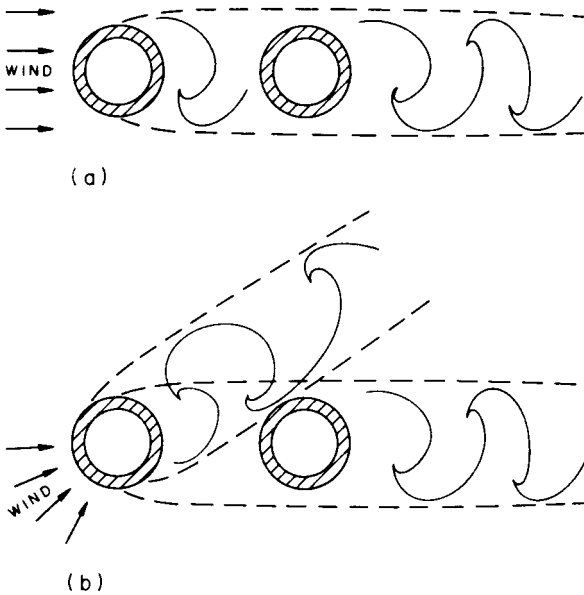


FIGURE 29.18 Buffeting by the wake of an upstream structure.

divergence. All types of instability feature a sudden start at a critical wind velocity and a rapid increase of violent displacements with wind velocity (Fig. 29.17C).

These various forms of excitation are briefly discussed in this chapter. Because all types of oscillations are influenced strongly by the properties of the wind, some basic wind characteristics are described first.

BASIC WIND CHARACTERISTICS

Wind is caused by differences in atmospheric pressure. At great altitudes, the air motion is independent of the roughness of the ground surface and is called the *geostrophic*, or *gradient* wind. Its velocity is reached at a height called *gradient height*, which lies between about 1000 and 2000 ft. Below the gradient height, the flow is affected by surface friction, by the action of which the flow is retarded and turbulence is generated. In this region, known as the *planetary boundary layer*, the three components of wind velocity resemble the traces shown in Fig. 29.19. The longitudinal component consists of a mean plus an irregular turbulent fluctuation; the lateral and vertical components consist of similar fluctuations. These turbulent motions can be characterized in a number of different ways.

The longitudinal motion at height z can be expressed as

$$V_z(t) = \bar{V}_z + v(t) \quad (29.23)$$

where \bar{V}_z = mean wind velocity (the bar denotes time average) and $v(t)$ = fluctuating component.

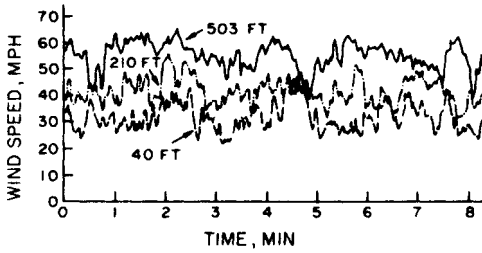


FIGURE 29.19 Record of horizontal component of wind speed at three heights on 500 ft mast in open terrain. (Courtesy of E. L. Deacon.)

Mean Wind Velocity. The mean wind velocity \bar{V}_z varies with height z as represented by the mean wind velocity profile (Fig. 29.20). The profiles observed in the field can be matched by a logarithmic law, for which there are theoretical grounds, or by an empirical power law

$$\frac{\bar{V}_z}{\bar{V}_G} = \left[\frac{z}{z_G} \right]^\alpha \tag{29.24}$$

where \bar{V}_G = gradient wind velocity, z_G = gradient height, and α = an exponent <1 . Gradient height z_G and exponent α depend on the surface roughness, which can be characterized by the surface drag coefficient κ (here referenced to the wind speed at 10 meters).

A few typical values of these parameters are given in Fig. 29.20. The mean wind profiles shown are characteristic of level terrain. They can significantly change, par-

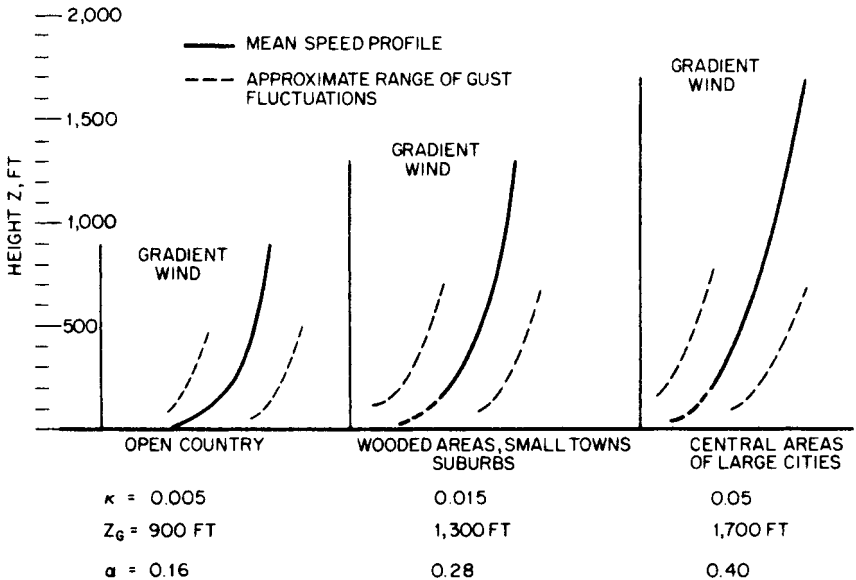


FIGURE 29.20 Vertical profiles of mean wind velocity for three typical terrains.

ticularly in the lower region, when the air flow meets an abrupt change in surface roughness or terrain contour. A sudden increase in roughness reduces the wind speed near the ground while a hill accelerates the flow over its crest.

The mean wind profiles are useful when predicting the wind speed at a particular site. The gradient wind speed is estimated using data registered by the nearest meteorological stations at their standard height, which is usually 33 ft (10 meters). The mean wind velocity generally depends on the period over which the wind speed is averaged. Periods from 10 to 60 minutes appear adequate for engineering considerations and usually yield reasonably steady mean values. The same duration is suitable to define the fluctuating wind component.

Fluctuating Components of the Wind. The fluctuating components of the wind change with height less than the mean wind and are random both in time and space. The random nature of the wind requires the application of statistical concepts (see Chap. 11). The basic statistical characteristics of the velocity fluctuations are the intensity of turbulence, the power spectral density (power spectrum), the correlation between velocities at different points, and the probability distribution.

The intensity of turbulence is defined as σ_v/\bar{V}_z , where $\sigma_v = \sqrt{\overline{v^2}(t)}$ is the root-mean-square (rms) fluctuation in the longitudinal direction. The intensity of the lateral and vertical fluctuations can be described similarly. For wind, the intensity of turbulence is between 5 and 25 percent. The magnitude σ_v also defines the probability distribution of the fluctuations which may be assumed to be Gaussian (normal).

The energy of turbulent fluctuations (gustiness) is distributed over a range of frequencies. This distribution of energy with frequency f can be described by the spectrum of turbulence (power spectral density) $W_v(f)$. The relationship between the spectrum and the variance is

$$\int_0^\infty W_v(f) df = \sigma_v^2$$

which leads to another form of the spectrum known as the *logarithmic spectrum* $fW_v(f)/\sigma_v^2$. This form of the spectrum is dimensionless and preserves the relative contributions to the variance at different frequencies represented on a logarithmic scale; and its integral is

$$\int_0^\infty \frac{fW_v(f)}{\sigma_v^2} d \ln f = 1$$

The two forms of spectra are sketched in Fig. 29.21. A generalization of wind spectra for different wind velocities is possible if the frequency scale is so modified

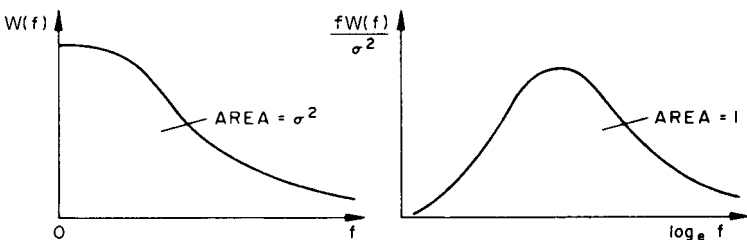


FIGURE 29.21 Two different ways of presenting power spectral densities.

that it too is dimensionless. The ratio $f\bar{V}$ is the so-called *inverse wavelength* related to the “size” of atmospheric eddies. This may be expressed as a ratio to a representative length scale L , such as the wavelength of the eddies at the peak of the spectrum. The dimensionless frequency or inverse wavelength may now be written

$$\bar{f} = fL/\bar{V}$$

Under certain circumstances this relationship is also known as the Strouhal number or the reduced frequency.

It is generally found that while the length scale L in the oncoming flow corresponds to that of the turbulence itself (this in the natural wind is of the order of thousands of feet), in the wake the governing length scale is of the same order as the diameter of the body D . This is illustrated in Fig. 29.22.

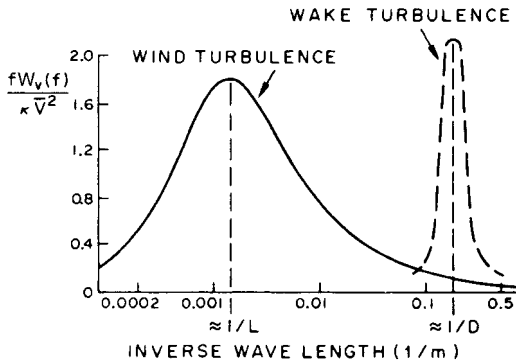


FIGURE 29.22 Universal spectrum of horizontal gustiness in strong winds and example of spectrum of fluctuations in wake.

The spectrum of horizontal gustiness in strong winds is largely independent of height above the ground, is proportional to both the surface drag coefficient κ and the square of the mean velocity at the standard height of 10 meters, \bar{V}_{10} , and can be represented, with some approximations, as^{6,7}

$$W_v(f) = 4\kappa\bar{V}_{10}^2 \frac{L/\bar{V}_{10}}{(2 + \bar{f}^2)^{5/2}} \tag{29.25}$$

in which f = frequency, Hz, $\bar{f} = fL/\bar{V}_{10}$ where L = scale length ≈ 4000 ft, and κ is given in Fig. 29.20. This spectrum is shown in Fig. 29.22.

The variance of the velocity fluctuations is

$$\sigma_v^2 = \int_0^\infty W_v(f) df = 6.68\kappa\bar{V}_{10}^2 \tag{29.26}$$

It can be seen from Eqs. (29.25) and (29.26) that large velocity fluctuations can be expected in rough terrain where coefficient κ is large.

The spatial correlation of wind speeds at two different stations is described by the coherence function (see Chap. 22),

$$\gamma_{12}^2(f) = \frac{|W_{12}(f)|^2}{W_1(f)W_2(f)} \leq 1 \quad (29.27)$$

where $W_{12}(f)$ = cross spectrum (generally complex) between stations 1 and 2; $W_1(f)$ and $W_2(f)$ are power spectra of the two stations. The coherence function depends primarily on the parameter $\Delta z f / \bar{V}$, where Δz = separation and $\bar{V} = \frac{1}{2}(\bar{V}_1 + \bar{V}_2)$ is the average wind speed. A suitable approximate function is

$$\sqrt{\text{Coherence}} = e^{-c(\Delta z f / \bar{V})}$$

where c is a constant having a value of approximately 7 for vertical separation and approximately 15 for horizontal separation. Coherence decreases with both separation and frequency. A more detailed discussion of wind characteristics is given in Refs. 1 and 7.

EXCITATION DUE TO TURBULENCE

When a structure is exposed to the effects of wind, the fluctuating wind velocity translates into fluctuating pressures, which in turn produce a time-variable response (deflection) of the structure. This response is random and represents the basic type of wind-induced oscillations. The theoretical prediction of this oscillation is rather complex but can be reduced to a simple procedure suitable for design purposes. The discussion of the oscillation is therefore presented in two parts. In the first part, the basic theoretical steps are outlined. In the second part, the design procedure known as the gust-factor approach is given in more detail.

FUNDAMENTALS OF RESPONSE PREDICTION

If the area A of the structure exposed to wind is small relative to the significant turbulent eddies, the so-called *quasi-steady theory* for turbulence can be used to estimate aerodynamic forces. In the drag direction, the drag force

$$\begin{aligned} D(t) &= \frac{1}{2} \rho C_D A V^2(t) \\ &= \frac{1}{2} \rho C_D A \bar{V}^2 \left[1 + 2 \frac{v(t)}{\bar{V}} + \frac{v^2(t)}{\bar{V}^2} \right] \end{aligned}$$

where ρ = air density (normally equal to 0.0024 slugs/ft³), and C_D = drag coefficient. If $v(t) \ll \bar{V}$, the squared term is ignored. The spectra of the fluctuating drag and velocity are then related as

$$\frac{W_D(f)}{\bar{D}^2} = 4 \frac{W_v(f)}{\bar{V}^2} \quad (29.28)$$

where the mean drag (static component of the drag) is

$$\bar{D} = \frac{1}{2} \rho C_D A \bar{V}^2 \quad (29.29)$$

and $W_v(f)$ is given by Eq. (29.25).

With large bodies, the wavelength is comparable to the size of the body itself (that is, $f\sqrt{A}/\bar{V} \approx 1$) and it is necessary to modify the drag spectrum by the so-called *aerodynamic admittance function* $|X_{aero}(f)|^2$. This function⁶ describes the modifying influence of any changes in effective drag coefficient as well as the decrease in correlation of the eddies as the wavelength of the eddies approaches the diameter of the body. Thus, the modified drag spectrum is

$$\frac{W_D(f)}{\bar{D}^2} = 4|X_{aero}(f)|^2 \frac{W_v(f)}{\bar{V}^2}$$

If these forces act on an elastic spring-mass-damper system, the response of this system u will have a spectrum

$$\frac{W_u(f)}{\bar{u}^2} = |X_{aero}|^2 |X_{mech}|^2 \frac{4W_v(f)}{\bar{V}^2}$$

where static deflection $\bar{u} = \bar{D}/k$, k = stiffness constant, and the mechanical admittance function is

$$|X_{mech}|^2 = \frac{1}{[1 - (f/f_n)^2]^2 + 4\zeta^2(f^2/f_n^2)}$$

where ζ = critical damping ratio, and f_n = natural frequency of the system.

The transition from the spectrum of the wind-velocity fluctuations to the spectrum of the response is shown diagrammatically in Fig. 29.23. The variance of the response σ_u^2 is obtained from the spectrum of the response,

$$\sigma_u^2 = \int_0^\infty W_u(f) df \tag{29.30}$$

The relationships above describe the mean and the variance of the response. For engineering purposes, it is also useful to define extreme values. It is often satisfactory to assume that the process in question is Gaussian with probability density function given by

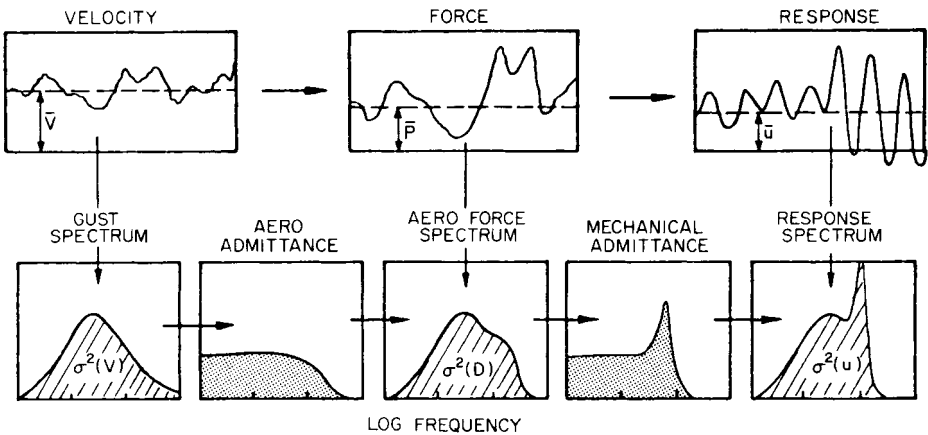


FIGURE 29.23 Transition from gust spectrum to response spectrum.

$$p(u) = \frac{1}{\sqrt{2\pi} \sigma_u} e^{-(u - \bar{u})^2/2\sigma_u^2}$$

This distribution is fully described by the mean and the variance. Maximum values of the response during time T can be written as

$$u_{\max} = \bar{u} + g\sigma_u \tag{29.31}$$

where g = peak factor. The average largest value of the peak factor in a period T can be estimated from⁶

$$g = \sqrt{2 \ln \nu T} + \frac{0.5772}{\sqrt{2 \ln \nu T}} \tag{29.32}$$

where ν is an effective cycling rate of the process, generally close to the natural frequency. The relationship of the distribution of the largest peak value to the distribution of all values is shown in Fig. 29.24. As can be seen, when the period T or the natural frequency increases, the expected peak displacement also increases. The factor g usually ranges between 3 and 5.

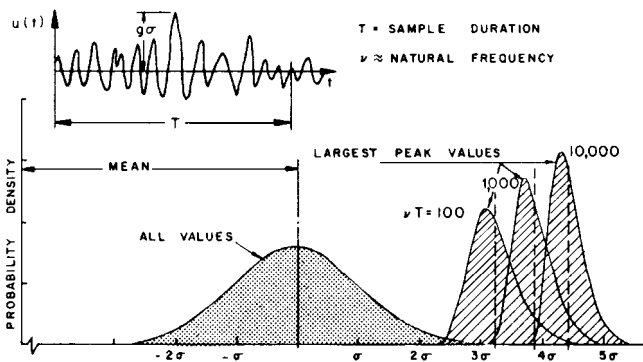


FIGURE 29.24 Relationship of distribution of largest peak value to distribution of all values (for a stationary random process).

Further extension of the concept includes the cross correlation of the wind loads at different stations (e.g., heights), the shape of the vibration mode, and the nonuniformity of the mean flow. These factors can be included into the solution formulated in terms of modal analysis (see Chap. 21). With a prismatic structure, the displacement may be expressed in the form

$$u(z,t) = \sum_{j=1}^{\infty} q_j(t)\phi_j(z) \tag{29.33}$$

where $q_j(t)$ = the generalized coordinate of the j th mode, and $\phi_j(z)$ = the j th mode of natural vibrations to an arbitrary scale.

With damping small and natural frequencies well separated, the cross correlation of the generalized coordinate can be neglected and the mean-square displacement (the variance) is

$$\overline{u^2(z,t)} = \sum_{j=1}^{\infty} \overline{q_j^2} \phi_j^2(z) \tag{29.34}$$

The variance of the generalized coordinate $\overline{q_j^2}$ is determined by the power spectrum of the generalized force Q_j . When the lateral dimension of the structure is small, only cross correlation in direction z need be considered. Then the power spectrum of the generalized force is

$$W_{Q_j}(f) = \int_0^H \int_0^H W_{12}(z_1, z_2, f) \phi_j(z_1) \phi_j(z_2) dz_1 dz_2 \tag{29.35}$$

where $W_{12}(z_1, z_2, f)$ = cross spectrum of the wind loads at heights z_1 and z_2 , and H = height of the structure. With respect to Eq. (29.28), the cross spectrum of the wind loads can be expressed in terms of the power spectrum of the wind speed [Eq. (29.25)] and the coherence function, Eq. (29.27).

The variance of q_j is

$$\begin{aligned} \overline{q_j^2} &= \int_0^{\infty} \frac{1}{(2\pi f_j)^4 M_j^2} \frac{1}{[1 - (ff_j)^2]^2 + 4\zeta^2 (ff_j)^2} W_{Q_j}(f) \\ &\approx \frac{1}{64\pi^3 \zeta_j^2 f_j^3 M_j^2} W_{Q_j}(f_j) + \frac{1}{(2\pi f_j)^4 M_j^2} \int_0^{f_j} W_{Q_j}(f) df \end{aligned} \tag{29.36}$$

where f_j = j th natural frequency and generalized mass

$$M_j = \int_0^H m(z) \phi_j^2(z) dz \tag{29.37}$$

where $m(z)$ = mass of the structure per unit length. The approximate integration⁸ of Eq. (29.36) yields the response composed of two parts, the resonance effect (the first term) and the background turbulence effect (the second term), as shown in Fig. 29.25. The variance of the displacement follows from Eq. (29.34), and its standard deviation (rms dynamic displacement) is $\sigma_u(z) = \sqrt{\overline{u^2(z,t)}}$. The peak response is established from Eq. (29.31) by means of the peak factor g [Eq. (29.32)] as in one degree-of-freedom. The mean deflection $\bar{u}(z)$ is the static deflection due to the mean wind \bar{V}_z .

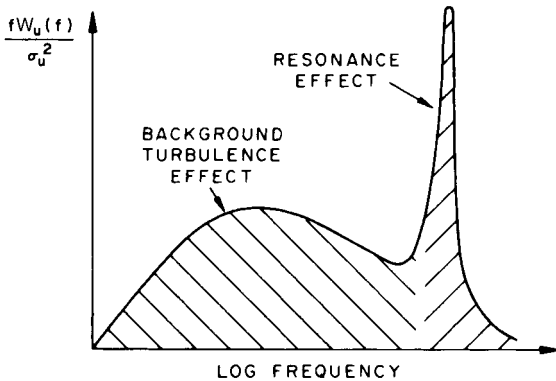


FIGURE 29.25 Spectrum of structural response with indication of resonance effect and background turbulence effect.

Other analyses of slender structures are also available.⁹⁻¹¹ In applications to buildings and free-standing towers, the analysis can usually be limited to the first modal component in Eq. (29.34). Application to buildings and structures with significant lateral dimension requires the incorporation of the horizontal cross correlation as well. A complete solution established by means of simplifying assumptions and numerical integrations is given below.

GUST-FACTOR APPROACH

The gust-factor approach is a design procedure derived on the basis of the theory above by means of a few simplifying assumptions. The approach given here is a modified version of the method described in Ref. 12 and adopted in Ref. 13. It considers only the response in the first vibration mode which is assumed to be linear. These assumptions are particularly suitable for buildings. The method yields all the data needed in design: the maximum response, the equivalent static wind load that would produce the same maximum response, and the maximum acceleration needed for the evaluation of the physiological effects of strong winds (human comfort).

The gust factor G is defined as the ratio of the expected peak displacement (load) in a period T to the mean displacement (load) \bar{u} . Hence, the maximum expected response is

$$u_{\max} = G\bar{u} = \left(1 + g \frac{\sigma_u}{\bar{u}}\right) \bar{u} \quad (29.38)$$

The gust factor is given as

$$G = 1 + g \sqrt{\frac{K}{C_e} \left(B + \frac{sF}{\zeta}\right)} \quad (29.39)$$

where ζ = damping ratio and K = factor related to the surface roughness; this factor is equal to 0.08 for open terrain (zone A), 0.10 for suburban, urban, or wooded terrain (zone B), and 0.14 for concentrations of tall buildings (zone C). All the other parameters appearing in Eq. (29.39) can be obtained from Fig. 29.26. C_e = exposure factor based on the mean wind speed profile (coefficient α) and thus on surface roughness. For the three zones, the exposure factor is obtained from Fig. 29.26A for the height of the building H . C_e relates to wind pressure rather than speed. Hence, the mean wind speed at the top of the building is given by

$$\bar{V}_H = \bar{V}_{10} \sqrt{C_e}$$

where \bar{V}_{10} = reference wind speed at the standard height of 10 meters. \bar{V}_{10} can be obtained from meteorological stations. Velocity \bar{V}_H is needed for determination of parameters s and F . Factors B , s , F , and g are given in Fig. 29.26C to f as a function of parameters indicated; D = width of the frontal area, and f_n = the first natural frequency of the structure in cycles per second. The average fluctuation rate v , on which the peak factor g depends, is evaluated from the formula

$$v = f_0 \sqrt{\frac{sF/\zeta}{B + sF/\zeta}} \quad (29.40)$$

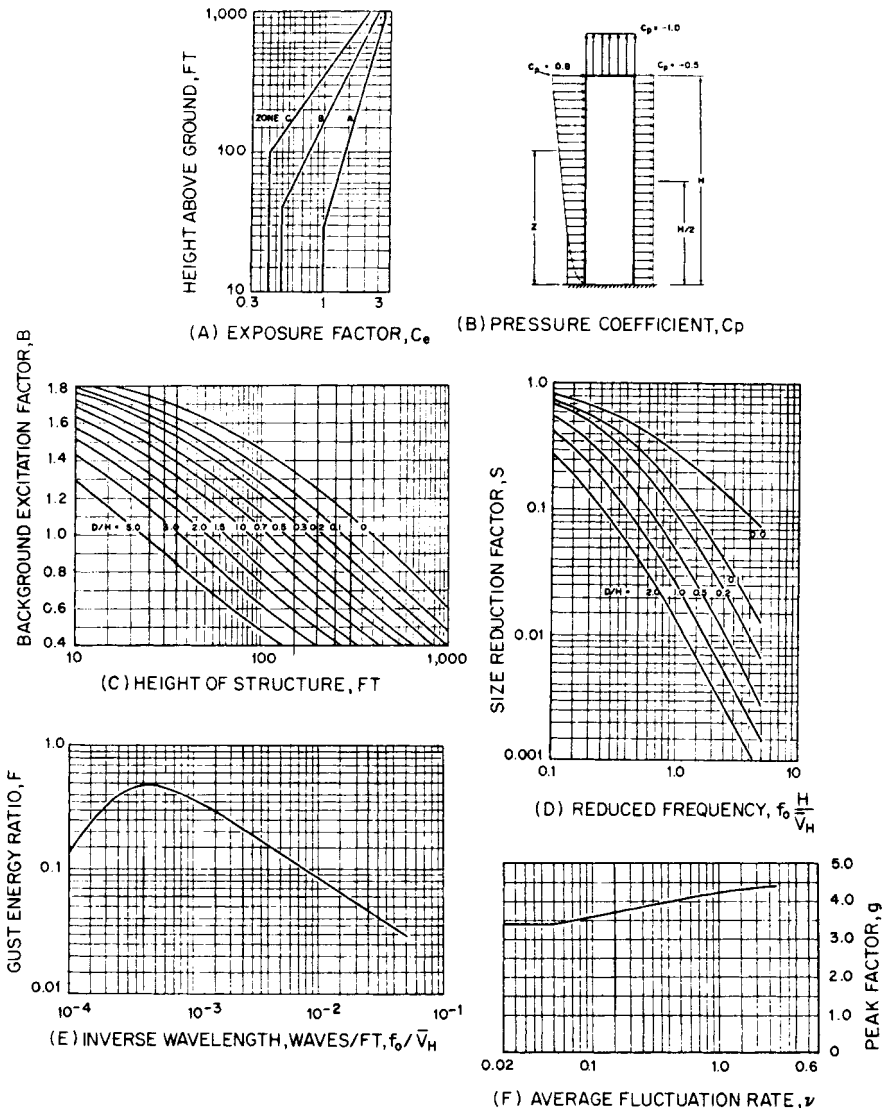


FIGURE 29.26 Components of gust factor.

The peak factor g is plotted in Fig. 29.26F, assuming a period of observation $T = 3600$ sec; it can also be calculated from Eq. (29.32).

The parameters given also yield the design wind pressure p , which produces displacement u_{max} if applied as a static load. This design pressure

$$p = qC_eGC_p \tag{29.41}$$

where $q = \frac{1}{2}\rho\bar{V}_{10}^2$ is the reference mean-velocity pressure, and $C_e =$ exposure factor. In this case, C_e varies continuously with the elevation according to Fig. 29.26A for pressures acting on the windward face of the structure; for the leeward face, C_e is constant and evaluated at one-half the height of the building. The quantity $C_p =$ average pressure coefficient, which depends on the shape of the structure and the flow pattern around it. For a typical building with a flat roof and a height greater than twice the width, the coefficients are given for the windward and leeward faces in Fig. 29.26B together with the pressure distribution.

The peak acceleration A of a structure due to gusting wind is given by

$$A = u_{\max} \frac{4\pi^2 f_0^2 g}{G} \sqrt{\frac{KsF}{C_e \zeta}}$$

where $u_{\max} =$ maximum deflection under the design pressure p . The other parameters are equal to those used in Eq. (29.39). When the acceleration exceeds about 1 per cent of gravity, the motion is usually perceptible. However, there are large differences in the perceptibility of motions having very low frequencies.^{14,15} Similar approaches are given in Refs. 16 to 18.

EFFECT OF GUSTS ON CLADDING AND WINDOWS

Wind gusts produce local pressures on cladding and window panels of a building. Because the natural frequency of such a panel is very high compared with the frequency components of the wind-speed fluctuations, the panel displacement is essentially static. Its design may be based on the static displacement resulting from maximum expected pressure, which is the algebraic sum of the height and time-dependent exterior pressure (or suction) and the constant interior pressure (or suction). If the fluctuating component of the pressure $p(t)$ is considered to be a stationary random process, the exterior expected maximum pressure is

$$p_{\max} = \bar{p} \left(1 + g \frac{\sigma_p}{\bar{p}} \right) = \bar{p} G \tag{29.42}$$

where $\bar{p} = \frac{1}{2}\rho C_p \bar{V}^2 =$ mean pressure

$C_p =$ local pressure coefficient

$\sigma_p =$ standard deviation of the fluctuating pressure component

$g =$ peak factor given by Eq. (29.32)

$G =$ gust factor

To account for the sensitivity of glass to both static and dynamic fatigue, it has been suggested^{19,20} that g or G in Eq. (29.42) be multiplied by a wind-on-glass effect factor.

Factors g , σ_p/\bar{p} , and C_p are most reliably determined from wind-tunnel experiments. They strongly depend on location of the panel, wind direction, turbulence intensity, and the local flow pattern determined by the shape of the building and its immediate environment. In full-scale experiments, values of g in excess of 10 have been observed in highly intermittent flow. Largest local pressure coefficients C_p (actually suction) appear with skew wind at the leading edge of the building where a typical value is $C_p = -1.5$. In that part of the building exposed to free flow, a gust factor $G \approx 2.5$ is a reasonable estimate.^{13,21} The interior pressure is not very high, but its magnitude and sign depend on openings and leakage.

Damage to windows may result from local wind pressure, but it also depends on material properties of glass and its fatigue. The fatigue limit of glass is only about 20 percent of the instantaneous strength.²⁰

VIBRATION DUE TO VORTEX SHEDDING

Vortex shedding represents the second most important mechanism for wind-induced oscillations. Unlike the gusts, vortex shedding produces forces which originate in the wake behind the structure, act mainly in the across-wind direction, and are, in general, rather regular. The resultant oscillation is resonant in character, is often almost periodic, and usually appears in the direction perpendicular to that of the wind. Lightly damped structures such as chimneys and towers are particularly susceptible to vortex shedding. Many failures attributed to vortex shedding have been reported.

When a bluff body is exposed to wind, vortices shed from the sides of the body creating a pattern in its wake often called the *Karman vortex street* (Fig. 29.16). The frequency of the shedding, nearly constant in many cases, depends on the shape and size of the body, the velocity of the flow, and to a lesser degree on the surface roughness and the turbulence of the flow. If the cross section of the body is noncircular, it also depends on the wind direction. The dominant frequency of vortex shedding f_s is given by

$$f_s = S \frac{\bar{V}}{D} \text{ Hz} \quad (29.43)$$

where S = dimensionless constant called the Strouhal number, \bar{V} = mean wind velocity, and D = width of the frontal area. The second dimensionless parameter is the Reynolds number $R = \bar{V}D/\nu$, where ν = kinematic viscosity. For air under normal conditions, $\nu = 1.6 \times 10^{-4}$ ft²/sec.

For a body having a rectangular or square cross section, the Strouhal number is almost independent of the Reynolds number. For a body having a circular cross section, the Strouhal number varies with the regime of the flow as characterized by the Reynolds number. There are three major regions: the subcritical region for $R \lesssim 3 \times 10^5$, the supercritical region for $3 \times 10^5 \lesssim R \lesssim 3 \times 10^6$, and the transcritical region for $R \gtrsim 3 \times 10^6$. Approximate values of the Strouhal number for typical cross sections are given in Table 29.2. The numbers given in this table are based on Refs. 1, 22, 23, and 24 and other measurements, and may be used for turbulent shear flow.

PREDICTION OF VORTEX-INDUCED OSCILLATION

Although the mechanism of vortex shedding and the character of the lift forces have been the subject of a great number of studies,²⁵ the available information does not permit an accurate prediction of these oscillations. The motion is most often viewed as forced oscillation due to the lift force, which, per unit length, may be written as

$$F_L = \frac{1}{2} \rho D \bar{V}^2 C_L(t) \quad (29.44)$$

TABLE 29.2 Aerodynamic Data for Prediction of Vortex-Induced Oscillations in Turbulent Flow

Cross section	Strouhal number S	rms lift coefficient σ_L	Bandwidth B	Correlation length L (diameters)
Circular:				
Subcritical	0.2	0.5	0.1	2.5
Supercritical	Not marked	0.14	Not marked	1.0
Transcritical	0.25	0.25	0.3	1.5
Square:				
Wind normal to face	0.11	0.6	0.2	3

where $C_L(t)$ is a lift coefficient fluctuating in a harmonic or random way. Some authors^{26,27} consider vortex shedding to be self-excitation, which does not seem necessary, however, for relatively small motions. Hence, the solution of the response depends on the time-history assumed for $C_L(t)$.

HARMONIC EXCITATION OF PRISMATIC CYLINDERS BY VORTICES

Harmonic excitation represents a traditional model for vortex excitation, but it is really justified only for very low Reynolds numbers ($\lesssim 300$) or possibly for large vibration where the motion starts controlling both the wake and the lift forces in the form of the “locking-in” phenomenon. Strongest oscillations arise at that wind velocity for which the frequency of vortex shedding f_s is equal to one of the natural frequencies of the structure f_j . This resonant wind velocity is, from Eq. (29.43),

$$V_c = \frac{1}{S} f_j D \quad (29.45)$$

With free-standing towers and stacks, resonance in the first two modes is met most often; resonance with higher modes has been observed as well with guyed towers (Fig. 29.27).

At the resonant wind velocity, the lift force is given by Eq. (29.44) in which $C_L(t) = C_L \sin 2\pi f_j t$, and C_L = amplitude of lift coefficient. Assuming a uniform wind profile and a constant diameter D , the resonant amplitude of mode j at the critical wind velocity V_c is, from Eq. (29.33),

$$u_j(z) = \frac{\rho C_L}{16\pi^2 S^2} \frac{D^3}{\zeta M_j} \phi_j(z) \int_0^H \phi_j(z) dz \quad (29.46)$$

where M_j is given by Eq. (29.37) and ζ = structural damping ratio. The formula can be further simplified if it is assumed that the lift force is distributed along the structure in proportion to the mode $\phi_j(z)$. This assumption reflects the loss of spanwise correlation of the forces. Then, with constant mass per unit length $m(z) = m$, the resonant amplitude at the height where the modal displacement is maximum:

$$u_j = \frac{\rho C_L}{16\pi^2 S^2} \frac{D^3}{\zeta m} \quad (29.47)$$

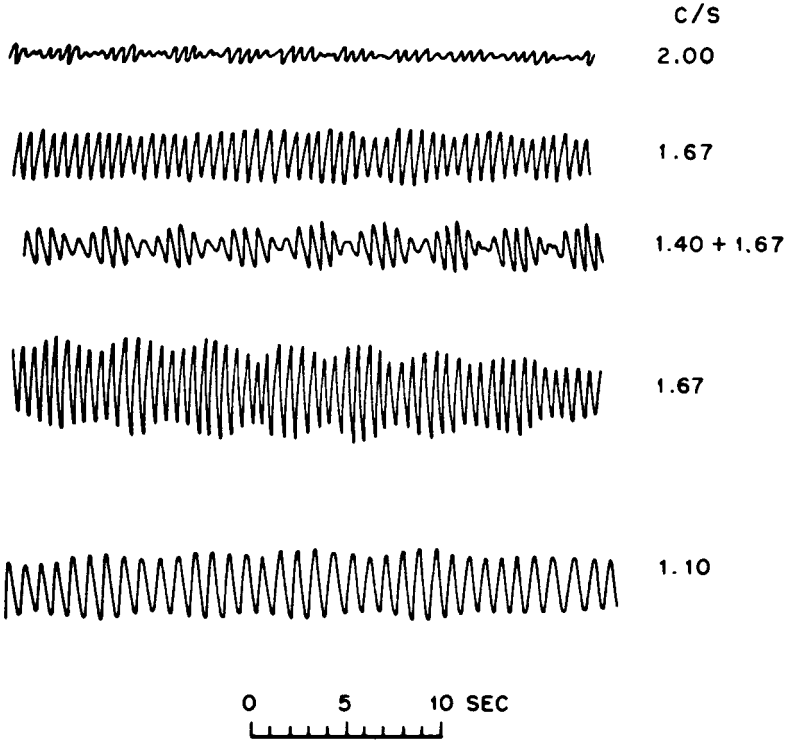


FIGURE 29.27 Vortex-induced oscillations in different modes measured on 1000 ft guyed tower.²⁸

For the first mode of a free-standing structure, this occurs at the tip. In higher modes, this amplitude appears at the height where local resonance takes place. For circular cylinders, a design value of the lift coefficient C_L is about $\sqrt{2}\sigma_L$. This simple formula can be used for the first estimate of the amplitudes that are likely to represent the upper bound. It is also indicative of the role of the diameter, mass, and damping of the structure. Approximate values of σ_L are given in Table 29.2.

RANDOM EXCITATION OF PRISMATIC CYLINDERS BY VORTICES

Even when vortex shedding appears very regular, the lift force and thus $C_L(t)$ are not purely harmonic but random. The power spectrum of the lift force per unit length is from Eq. (29.44).

$$W_L(f) = \left(\frac{1}{2} \rho D \bar{V}^2 \sigma_L \right)^2 W_L'(f) \tag{29.48}$$

where $\sigma_L = \sqrt{\overline{C_L^2(t)}}$ is the standard deviation of the lift coefficient and $W_L'(f) =$ normalized power spectrum of $C_L(t)$ for which

$$\int_0^\infty W_L'(f) df = 1 \tag{29.49}$$

With circular cylinders, the lift force is narrow-band random in the subcritical and transcritical^{22,23} ranges where the energy is distributed about the dominant frequency f_s , given by Eq. (29.43) (Fig. 29.28A). Such spectra can be described by a Gaussian-type curve,

$$W_L'(f) = \frac{1}{\sqrt{\pi B f_s}} \exp \left[- \left(\frac{1 - f/f_s}{B} \right)^2 \right] \tag{29.50}$$

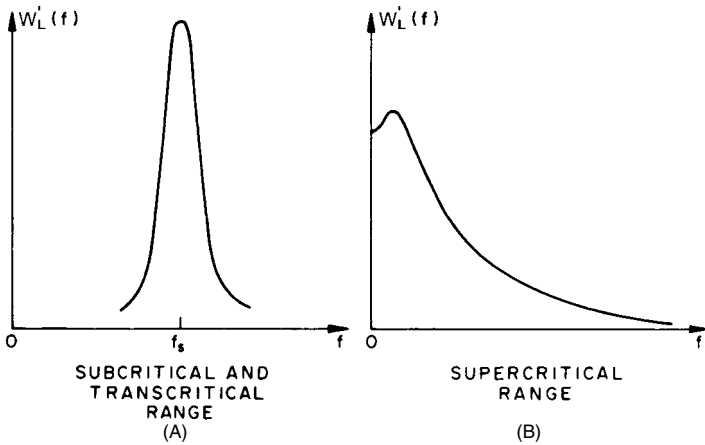


FIGURE 29.28 Spectra of lift coefficient for circular cylinder.

A few design values of bandwidth B are given in Table 29.2. In the supercritical range, the power spectrum is broad (Fig. 29.28B) and can be expressed as²⁹

$$W_L'(f) = 4.8 \frac{1 + 682.2(fD/\bar{V})^2}{[1 + 227.4(fD/\bar{V})^2]^2} \frac{D}{\bar{V}} \tag{29.51}$$

Because the vortices are three-dimensional, a realistic treatment also requires the inclusion of the spanwise cross correlation of the lift forces. This can be done in terms of the “correlation length” L given in number of diameters.

Approximate values of L are given in Table 29.2. The correlation length decreases with turbulence³⁰ and shear, and increases with aspect ratio $2H/D$ and the amplitude of the motion as shown in Fig. 29.29.

Using the correlation length, the spectral density of the lift force, Eqs. (29.50) and (29.51), and a few further approximations, the vibration can be evaluated from Eqs. (29.34) to (29.36). The root-mean-square (rms) displacement at height z in mode j is approximately

$$\sqrt{u_j^2(z,t)} = \frac{\pi^{1/4} \sigma_L \rho D^4 \phi_j(z/H)}{\sqrt{B} \zeta (4\pi S)^2 M_j} C$$

where

$$C^2 = \frac{(H/D)^2}{1 + (H/2LD)} \int_0^1 \left(\frac{z}{H}\right)^{3\alpha} \phi_j^2\left(\frac{z}{H}\right) d\left(\frac{z}{H}\right)$$

Here, α = wind profile exponent (Fig. 29.20), and parameters S , σ_L , B , and L are given in Table 29.2. The mode $\phi_j(z/H)$ is dimensionless, and consequently M_j is in slugs in this case. The peak response is $g \sqrt{u_j^2(z,t)}$, where the peak factor g is given by Eq. (29.32). If it is larger than about 2 percent of diameter D , locking-in may develop and the analysis should be repeated assuming harmonic excitation or at least random excitation with a significantly increased correlation length, as Fig. 29.29 indicates.

RANDOM EXCITATION OF TAPERED CYLINDERS BY VORTICES

Tapered cylinders, such as stacks, also vibrate due to vortex shedding, but less is known about the mechanism of excitation. It appears that the lift forces are narrowband random with a rather small correlation length L and with the dominant frequency f_s given by Eq. (29.43). As the diameter is variable, local resonance between f_s and the natural frequency f_j takes place at different heights z_r . As the wind speed increases, the resonance first appears at the tip and shifts downward. The critical wind speed for each height follows from Eq. (29.45) with $D = D(z_r)$. The rms displacements at height H due to local resonance at height z_r can be obtained from an approximate formula,³²

$$\begin{aligned} &\sqrt{u_j^2(H,t)} \\ &= \sqrt{\frac{L}{2\pi^3\zeta\Psi}} \frac{\sigma_L \rho D^4(z_r) \phi_j(z_r)}{8S^2 M_j} \phi_j(H) \end{aligned}$$

where

$$\Psi = \frac{dD(z_r)}{dz} + \frac{\alpha D(z_r)}{z_r}$$

or with a constant taper

$$\Psi = \frac{t}{H} + \frac{\alpha D(z_r)}{z_r}$$

where $t = D(0) - D(H)$ and α = the wind-profile exponent. The other parameters can be taken from Table 29.2. The values listed for the transcritical region may be adequate, inasmuch as most tapered stacks are large. The peak displacement is again obtained by means of the peak factor given by Eq. (29.32).

Maximum response of chimneys in the first mode usually results from local resonance at about $\frac{1}{4}H$. The height of maximum excitation follows from the condition $d[D^4(z)\phi_j(z)]/dz = 0$.

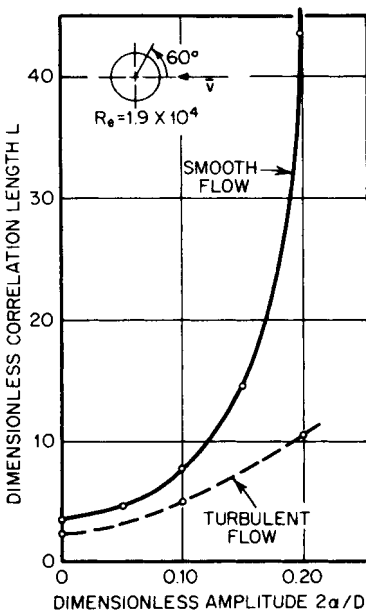


FIGURE 29.29 Variation of correlation length of vortex shedding with amplitude of motion and turbulence ($2a$ = double amplitude, turbulence intensity 10 percent).

SUPPRESSION OF VORTEX-INDUCED VIBRATIONS

Vortex shedding may induce severe vibration of a cylindrical structure such as a chimney, free-standing tower, guyed mast, bridge columns, etc. Very strong oscillations have been observed^{28,31} in all-welded structures where the damping ratio is extremely low, sometimes less than 0.005.^{8,28} Welded structures are particularly prone to fatigue failure, as the endurance limit may be only a fraction of the strength if heavy notches, flaws, attachments, or other adverse details are present. In other cases, the motion is intolerable because of its physiological effects or swaying of antennas. For these reasons, suppression of vibration is often desirable.

In some cases, vibration can be reduced by increasing the structural damping. This can be accomplished by additional dampers attached to an independent support²⁸ or to a special mass suspended from the structure and suitably tuned or by hanging chains³³ (see Chap. 6). Columns of a few bridges were filled with gravel, sand, or plastic balls partly filled with oil. The increase in mass may be unfavorable but can increase the original structural damping.

Another successful method of vibration control is to break down the wake pattern by providing the surface by helical “strakes” or “spoilers.”^{28,31,34} A suitable height of the spoilers is about $0.1D$ or more with a pitch of about $5D$. A significant drawback of the spoilers is that they considerably increase the drag, sometimes by 100 percent or more.^{31,35}

WAKE BUFFETING

If one structure is located in the wake of another, vortices shed from the upstream structure may cause oscillation of the downstream structure.^{36,37} If the two structures differ greatly in size or shape, this excitation is usually not significant. Strong vibration of the downstream structure may arise when two or more structures are identical and less than about 10 diameters apart. Then the structure in the wake is efficiently excited by well-tuned wake buffeting and its own vortex shedding. Such excitation has been observed with stacks and bridges, and to a certain degree with hyperbolic cooling towers.³⁶

GALLOPING OSCILLATIONS

Vibrations due to turbulence and vortices discussed above are induced by aerodynamic forces which are, to a high degree, independent of the motion and act even on stationary bodies. Quite a different kind of oscillation is induced by the aerodynamic forces generated by the motion itself. Such forces may result from oscillatory changes in pressure distribution brought about by the continuous change in the angle under which the wind strikes the structure (“angle of attack”). This kind of oscillation often has a tendency to diverge; it is called, summarily, *aerodynamic instability*, *flutter*, or *self-excited oscillation*. Sudden start and violent amplitudes are typical of such phenomena (Fig. 29.17C).

The mechanism of this oscillation is, in general, complex. The aerodynamic forces may be a function of the displacements (translation and rotation), vibration velocity, or both, and they may interact with turbulence and vortex shedding. The basic type of the self-excited oscillations is the lateral (across-wind) oscillation induced by

aerodynamic forces which are related to vibration velocity alone. Such oscillation is referred to as *galloping*. Typical features of galloping oscillation are motion in the direction perpendicular to that of the wind, sudden onset, large steady amplitudes increasing with wind velocity, and a frequency equal to the natural frequency. Galloping oscillation occurs in transmission lines and in a variety of structures having square, rectangular, or other sharp-edged cross sections.

The origin of galloping oscillation depends on the relation between lift and drag. If a body moves with a velocity \dot{u} in a flow having velocity \bar{V} perpendicular to its direction (Fig. 29.30), the aerodynamic force acting on the body is produced by relative wind velocity \bar{V}_{rel} . The angle of attack of relative wind is

$$\alpha = \arctan \frac{\dot{u}}{\bar{V}} \tag{29.52}$$

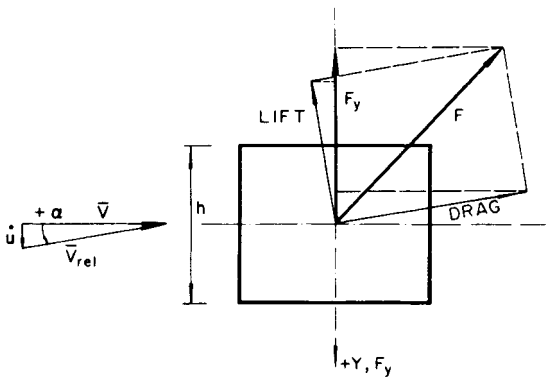


FIGURE 29.30 Cross section in flow.

The drag and lift components D and L of the aerodynamic force F are

$$D = C_D \frac{1}{2} \rho h l \bar{V}_{rel}^2$$

$$L = C_L \frac{1}{2} \rho h l \bar{V}_{rel}^2$$

where C_D and C_L are drag and lift coefficients at angle α (Fig. 29.31), h = depth of the cross section, and l = length of the body.

The component of force F into the direction of axis Y , therefore, is

$$F_y = -(C_D \sin \alpha + C_L \cos \alpha) \frac{1}{2} \rho h l \bar{V}^2 \sec^2 \alpha = C_{F_y} \frac{1}{2} \rho h l \bar{V}^2 \tag{29.53}$$

where

$$C_{F_y} = -(C_L + C_D \tan \alpha) \sec \alpha \tag{29.54}$$

The lateral force excites the vibration if the first derivative of C_{F_y} at $\alpha = 0$ is >0 , hence

$$A_1 = \left. \frac{dC_{F_y}}{d\alpha} \right|_{\alpha=0} = -\left(\frac{dC_L}{d\alpha} + C_D \right) > 0 \tag{29.55}$$

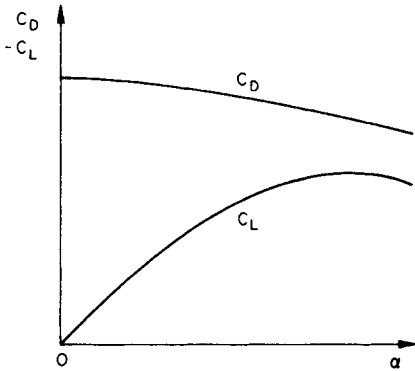


FIGURE 29.31 Lift and drag as function of angle of attack.

This condition for aerodynamic instability is known as *Den Hartog's criterion*.³⁸ Substitution of Eq. (29.52) into Eq. (29.54) indicates that the aerodynamic forces depend on vibration velocity and thus actually represent the aerodynamic damping. This damping is negative if $A_1 > 0$. Because the system also has structural damping ζ , which is positive, the vibration will start only if the total available damping becomes less than 0. This condition yields the onset (minimum) wind velocity for galloping from the equilibrium (or zero displacement) position as

$$\bar{V}_0 = \zeta \frac{2\pi f_j h}{nA_1} \tag{29.56}$$

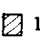





where f_j = natural frequency, $n = \rho h^2/(4m)$ = mass parameter, and m = mass of the body per unit length. Some values of coefficient A_1 are given in Table 29.3.

Gallopings oscillations starting from zero initial displacement can occur only when the cross section has $A_1 > 0$. Cross sections having $A_1 \leq 0$ are generally considered stable even though galloping may sometimes arise if triggered by a large initial amplitude.⁴¹

The response and the onset velocity are often very sensitive to turbulence. Some cross sections, such as a flat rectangle or a D section, are stable in smooth flow but can become unstable in turbulent flow.^{41,42} With other cross sections, turbulence may stabilize a shape that is unstable in smooth flow (see Table 29.2). From Eqs. (29.53) and (29.54) the nonlinear, negative aerodynamic damping can be calculated⁴³ for inclusion in the treatment of the across-wind response due to atmospheric turbulence.

The prediction of oscillations for wind velocities greater than V_0 depends on the shape of the C_{Fy} coefficient and requires the application of nonlinear the-

TABLE 29.3 Coefficients A_1 for Determination of Galloping Onset Wind Velocity (Infinite Prisms)

		Cross section (Side ratio)					
		Unstable in smooth flow			Stable in smooth flow		
		Square	Rect.	Rect.	Rect.	Rect.	D-section*
Flow	$V \rightarrow$	 1	 2	 1	 3	 2	 2
		1	3	2	2	1	1
Smooth		2.7	1.91	2.8	0	-0.03	-0.1
Turbulent ≈ 10 percent intensity		2.6	1.83	-2.0	0.74	0.17	0

* Varies with Reynolds number.

ory.³⁹⁻⁴² A few typical cases are shown in Fig. 29.32. The cases are typical of a square cross section, a flat rectangular section, and a D section whose angle of attack is allowed to change due to drag. Similar response can be expected with other cross sections.

Torsion can also participate in galloping oscillations and play an important part in the vibration. This is the case with angle cross sections⁴⁴ and bundled conductors.⁴⁵ The quasi-steady theory of pure torsional galloping can be found in Ref. 46. A solution of coupled galloping is presented in Ref. 47.

Gallopings often appears in overhead conductors which also vibrate due to vortex shedding. Vortex shedding produces resonant vibration in a high-vibration mode. Galloping usually involves the fundamental mode and is known to occur when the

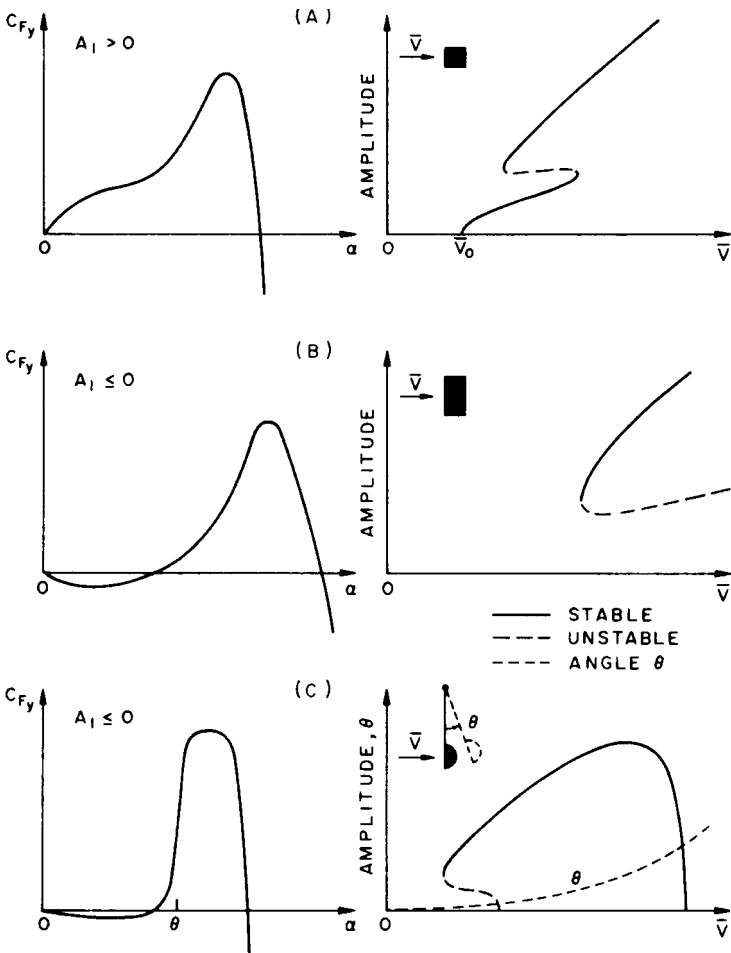


FIGURE 29.32 Typical lateral force coefficients C_{Fy} and corresponding galloping oscillations: (A) vibration from equilibrium position, (B) vibration triggered by initial amplitudes, and (C) vibration with variable angle of attack.

conductor is ice-coated or free of ice. The vibration often leads to fatigue failures, and various techniques are therefore used to reduce the amplitude. This can be achieved by means of resonant dampers⁴⁸ consisting of auxiliary masses suspended on short lengths of cable which dissipate energy through the bending (see Chap. 6), or aerodynamic dampers⁴⁹ consisting of perforated shrouds. Vibrations of bundled conductors can be eliminated by twisting the bundle⁴⁵ and thereby changing the aerodynamic characteristics in the spanwise direction.

VIBRATION OF SPECIAL STRUCTURES

The basic types of vibration discussed above are common in many structures. However, there are some special structures which would require individual treatment. A few examples are cited below.

Guyed towers experience complicated vibration patterns because of the nonlinearity of the guys, the three-dimensional character of the response, the interaction between the guys and the tower, and other factors.^{28,50-52}

Hyperbolic cooling towers can suffer from some of the effects of wake buffeting³⁶ and are susceptible to turbulence.⁵³

Information on the vibration of a number of special structures can be found in Refs. 2 to 5.

REFERENCES

1. Davenport, A. G., et al.: "New Approaches to Design against Wind Action," Faculty of Engineering Science, University of Western Ontario (unpublished).
2. *Proc. IUTAM-IAHR Symp. Karlsruhe*, 1972.
3. *Proc. Conf. National Physical Laboratory, Teddinton, Middlesex*, 1963.
4. *Proc. Intern. Res. Seminar, Ottawa*, 1967.
5. *Proc. 3d Intern. Conf.*, Tokyo, 1971.
6. Davenport, A. G.: *Inst. Civil Eng. Paper No. 6480*, 449-472 (August 1961).
7. Harris, R. I.: Seminar of Construction Industry Research and Information Association, paper 3, Institution of Civil Engineers, 1970.
8. Novak, M.: *Acta Tech. Czechoslovak Acad. Sci.*, **4**:375 (1967).
9. Vickery, B. J.: *J. Struct. Div. Am. Soc. Civil Engrs.*, **98**:21 (January 1972).
10. Davenport, A. G.: *Proc. Inst. Civil Engrs.*, **23**:449 (1962).
11. Etkin, B.: Meeting on Ground Wind Load Problems in Relation to Launch Vehicles, pp. 21.1-15, Langley Research Center, NASA, June 1966.
12. Davenport, A. G.: *J. Struct. Div., Am. Soc. Civil Engrs.*, **93**:11 (June 1967).
13. "Canadian Structural Design Manual 1970," Suppl. 4, National Research Council of Canada, 1970.
14. Chen, P. W., and L. E. Robertson: *J. Struct. Div. Am. Soc. Civil Engrs.*, **98**:1681 (August 1972).

15. Hansen, R. T., J. W. Reed, and E. H. Vanmarcke: *J. Struct. Div. Am. Soc. Civil Engrs.*, **99**:1589 (July 1973).
16. Vellozzi, Y., and E. Cohen: *J. Struct. Div. Am. Soc. Civil Engrs.*, **94**:1295 (June 1968).
17. Vickery, B.: U.S. Dept. of Commerce, *Nat. Bur. Std. Bldg. Sci., Ser.* **30**:93.
18. Simiu, E.: *J. Struct. Div. Am. Soc. Civil Engrs.*, **100**:1897 (September 1974).
19. Allen, D. E., and W. A. Dalgliesh: Preliminary Publication of IABSE Symposium on Resistance and Ultimate Deformability of Structures, pp. 279–285, Lisbon, 1973.
20. Dalgliesh, W. A.: *Proc. U.S.-Japan Res. Seminar Wind Effects Structures*, Kyoto, Japan, September 1974.
21. Dalgliesh, W. A.: *J. Struct. Div. Am. Soc. Civil Engrs.*, **97**:2173 (September 1971).
22. Roshko, A.: *J. Fluid Mech.*, **10**:345 (1961).
23. Cincotta, J. J., G. W. Jones, and R. W. Walker: Meeting on Ground Wind Load Problems in Relation to Launch Vehicles, pp. 20.1–35, Langley Research Center, NASA, 1966.
24. Novak, M.: Ref. 5, pp. 799–809.
25. Morkovin, M. V.: *Proc. Symp. Fully Separated Flows*, p. 102, ASME, 1964.
26. Nakamura, Y.: *Rept. Res. Inst. Appl. Mech., Kyushu University*, **17**(59):217 (1969).
27. Hartlen, R. T., and I. G. Currie: *J. Eng. Mech. Div. Am. Soc. Civil Engrs.*, **70**:577 (October 1970).
28. Novak, M.: *Proc. IASS Symp. Tower-Shaped Steel r.c. Structures*, Bratislava, 1966.
29. Fung, Y. C.: *J. Aerospace Sci.*, **27**(11):801 (1960).
30. Surry, D.: *J. Fluid Mech.*, **52**(3):543 (1972).
31. Wotton, L. R., and C. Scruton: Construction Industry Research and Information Association Seminar, Paper 5, June, 1970.
32. Vickery, B. J., and A. W. Clark: *J. Struct. Div. Am. Soc. Civil Engrs.*, **98**:1 (January 1972).
33. Reed, W. H.: Ref. 4, Paper 36, pp. 283–321.
34. Scruton, C.: National Physical Laboratory Note 1012, April 1963.
35. Novak, M.: Ref. 4, pp. 429–457.
36. Scruton, C.: Ref. 4, pp. 115–161.
37. Cooper, K. R., and Wardlaw, R. L.: Ref. 5, pp. 647–655.
38. Den Hartog: *Trans., AIEE*, **51**:1074 (1932).
39. Parkinson, G. V., and J. D. Smith: *Quart. J. Mech. Appl. Math.*, **17**(2):225 (1964).
40. Novak, M.: *J. Eng. Mech. Div. Am. Soc. Civil Engrs.*, **95**:115 (February 1969).
41. Novak, M.: *J. Eng. Mech. Div. Am. Soc. Civil Engrs.*, **98**:27 (February 1972).
42. Novak, M., and Tanaka, H.: *J. Eng. Mech. Div. Am. Soc. Civil Engrs.*, **100**:27 (February 1974).
43. Novak, M., and Davenport, A. G.: *J. Eng. Mech. Div. Am. Soc. Civil Engrs.*, **96**:17 (February 1970).
44. Wardlaw, R. L.: Ref. 4, pp. 739–772.
45. Wardlaw, R. L., K. R. Cooper, R. G. Ko, and J. A. Watts: *Trans. IEEE*, 1975.
46. Modi, V. J., and J. E. Slater: Ref. 2, pp. 355–372.
47. Blevins, R. D., and W. D. Iwan: *J. Appl. Mech.*, **41**, no. 4, 1974.
48. “Overhead Conductor Vibration,” Alcoa Aluminum Overhead Conductor Engineering Data, no. 4, 1974.
49. Hunt, J. C. R., and D. J. W. Richards: *Proc. Inst. Elec. Engrs.*, **116**(11):1869 (1969).

50. Davenport, A. G., and G. N. Steels: *J. Struct. Div. Am. Soc. Civil Engrs.*, **91**:43 (April 1965).
51. Davenport, A. G.: Engineering Institute of Canada, **3**:119 (1959).
52. McCaffrey, R. J., and Hartmann, A. J.: *J. Struct. Div. Am. Soc. Civil Engrs.*, **98**:1309 (June 1972).
53. Hashish, M. G., and Abu-Sitta, S. H., *J. Struct. Div. Am. Soc. Civil Engrs.*, **100**:1037 (May 1974).

CHAPTER 29, PART III

VIBRATION OF STRUCTURES INDUCED BY SOUND

John F. Wilby

INTRODUCTION

Vibration of structures due to interaction with a surrounding fluid can occur in a variety of ways. Parts I and II of this chapter are concerned with several fluid flow phenomena—waves, vortices, and wind—that induce vibration in an adjacent structure. The intent in Part III is to address the response of structures to acoustic and aeroacoustic excitations, where the term *aeroacoustic* includes sources, such as turbulent boundary layers, that have many characteristics similar to those of an acoustic field. The excitations can be deterministic or random in nature, as defined in Chap. 1, depending on the particular source.

Sound-induced vibration can result in sound radiation to other regions, acoustic fatigue (also known as sonic or high-cycle fatigue) of the structure being excited, or transmission of vibration to attached equipment causing malfunction or failure. Interest is often centered on aerospace applications where structures are lightweight and sound levels are high. In that case, there is the likelihood of damage to the primary structure of an aerospace vehicle, payloads in a launch vehicle, or the equipment mounted on the structure. However, structural vibration due to acoustic excitation occurs in a wide range of other environments including building damage and vibration of equipment in microelectronics manufacturing facilities.

Different acoustic and aeroacoustic sources will be described, followed by a discussion of methods for predicting linear and nonlinear response of structures to an acoustic or aeroacoustic excitation. Then, the problem of acoustic fatigue will be addressed. Finally, test methods for the measurement of structural response to acoustic and aeroacoustic excitations will be identified.

SOUND SOURCES

Acoustic and aeroacoustic pressure fields may be deterministic or random, stationary or nonstationary, and homogeneous or inhomogeneous (see definitions in

Chap. 1). *Deterministic pressures* are periodic or almost-periodic (see Chap. 22) and can be described by time-dependent functions, whereas *random pressures* can be described only in statistical terms (see Chap. 22). *Stationary pressure fields* have properties that, on the average, are invariant with time. That is not true of *nonstationary pressure fields*, which can include impulsive excitations such as blast waves and sonic booms. *Homogeneous pressure fields* have properties that, on the average, are the same at any location on a structure, whereas *inhomogeneous pressure fields* have properties that change with location. The term *aeroacoustic* is used here in a general sense to include sound produced by fluid flow or by interaction of flows with solid bodies, and fluctuating aerodynamic pressures such as those beneath a turbulent boundary layer. For convenience, and without loss of generality, both acoustic and aeroacoustic pressure fields will be referred to herein as *sound fields*.

One important characteristic of a sound field is that the fluctuating pressures are distributed over a large area, if not the entire surface, of the excited structure, and usually consist of a wide range of frequencies that includes several modes of vibration of the structure. The response of the excited structure depends on several properties of the sound field—sound pressure, frequency content, spatial distribution of pressure level and phase, and duration of exposure. The spatial characteristics of a random pressure field are best described in terms of the pressure cross-spectrum (see Chap. 22), although narrowband correlation functions have been used as equivalent representations (see Chap. 11). Sound pressures encountered in everyday life cover a range of many orders of magnitude. Thus, it is convenient to express them in terms of a logarithmic quantity called the sound pressure level, L_p , which is expressed in terms of decibels (dB) and is defined by

$$L_p = 10 \log \left[\frac{p_{\text{rms}}^2}{p_{\text{ref}}^2} \right] = 20 \log \left[\frac{p_{\text{rms}}}{p_{\text{ref}}} \right] \quad \text{dB} \quad (29.57)$$

where p_{rms} is the root-mean-square (rms) value of the sound pressure and p_{ref} is a reference pressure that has been established by international standard to be $p_{\text{ref}} = 20 \mu\text{Pa}$ in air. The common reference for underwater sound pressures is $p_{\text{ref}} = 1 \mu\text{Pa}$.

The range of sound pressure levels encountered in practice is demonstrated by the typical values listed in Table 29.4. The levels vary from 0 dB at the threshold of human hearing to 170 dB or more on some surfaces of aerospace vehicles, well above the threshold of pain for a human. Typical sound pressure levels near a busy highway are on the order of 80 dB, and noisy machinery can generate sound pressure levels of about 100 dB at the operator's position.

Structural response to sound is of interest in a variety of situations but, as indicated by Table 29.4, the most intense sound fields can be found in aerospace applications. Thus, aerospace vehicle sound sources are of special interest and provide a wide range of characteristics. The sources include the exhaust of jet and rocket engines, propellers and fans, powered lift devices, turbulent boundary layers, oscillating shock waves, and sonic booms.¹ In many cases, the pressure field is neither stationary nor homogeneous. However, it is often acceptable to assume stationarity and homogeneity when predicting the response of a structure, if the variations in space and time are gradual. There are exceptions to this assumption, for example, propeller noise where the pressure field is strongly inhomogeneous with the sound pressure levels being very high in the plane of rotation of the propeller and decreasing rapidly in the forward and aft directions. A survey of near-field pressure fields on flight vehicles can be found in Ref. 2.

TABLE 29.4 Typical Sound Pressure Levels for Different Environments

Sound pressure level L_p (dB re 20 μ Pa)	Environment
170	Jet noise on aircraft surface
160	Immediate hearing damage
140	Threshold of pain
120	Jet airplane takeoff at 1500 ft (500 m)
100	Punch press and wood planers at 3 ft (1 m)
90	Power mower at 3 ft (1 m)
80	Truck at 60 ft (20 m)
70	Automobile at 60 ft (20 m)
50	Conversation level, A-weighted, in a free field, at 3 ft (1 m)
40	Quiet residential neighborhood
20	Recording studio, A-weighted
0	Threshold of hearing

Although the following discussion on sound sources is directed toward aerospace vehicles, it should be viewed more generally in terms of sound-generating mechanisms that can be found in a wide range of situations. For example, the high-velocity gas exhaust from a pressure relief valve has acoustical characteristics similar to those of a jet engine exhaust. Axial fans in air-conditioning systems or gas-cooled nuclear reactors have similar noise-generating mechanisms to those of a turbofan engine. Also, regions of flow separation on an automobile can have characteristics that are similar to those for separated flow on an airplane.

JET AND ROCKET EXHAUSTS

Jet and rocket noise is generated by interaction between the turbulent exhaust of the jet or rocket engine and the surrounding air. At low exhaust velocities, below about 1000 ft/sec (300 m/sec), the acoustic power generated by the exhaust is proportional to the eighth power of the exhaust velocity, V_j . However, as the velocity increases the index decreases until, for rocket exhausts, where the exhaust velocity is of the order of 9000 ft/sec (2750 m/sec), the acoustical power is proportional to the third power of velocity. As the mechanical power of a rocket exhaust is also proportional to V_j^3 , the acoustical power of a rocket exhaust is usually expressed in terms of an efficiency factor η , which is the ratio of acoustical power W_a to mechanical power W_m . That is,

$$W_a = \eta W_m = 0.5\eta TV_j \quad (29.58)$$

where T is the thrust of the rocket engine. Typical values^{3,4} of the efficiency factor are usually in the range 0.5 to 1.0 percent.

Since jet noise levels are determined by the relative velocity between the exhaust and the surrounding air, the noise levels will decrease as the vehicle accelerates at takeoff or liftoff, the highest levels occurring when the vehicle is stationary. This variation of noise level with vehicle speed means that the noise levels are nonstationary, although they can be considered as stationary over short time periods.

Jet noise is strongly directional, with the highest sound pressure levels in the far field occurring at angles of 30 to 50° to the jet axis, the angle being dependent on the exhaust velocity. The situation is not so well defined in the near field, where the aircraft structure is located. Representative near-field pressure contours can be found in Refs. 4 to 7, and typical contours are shown in Fig. 29.33.⁷

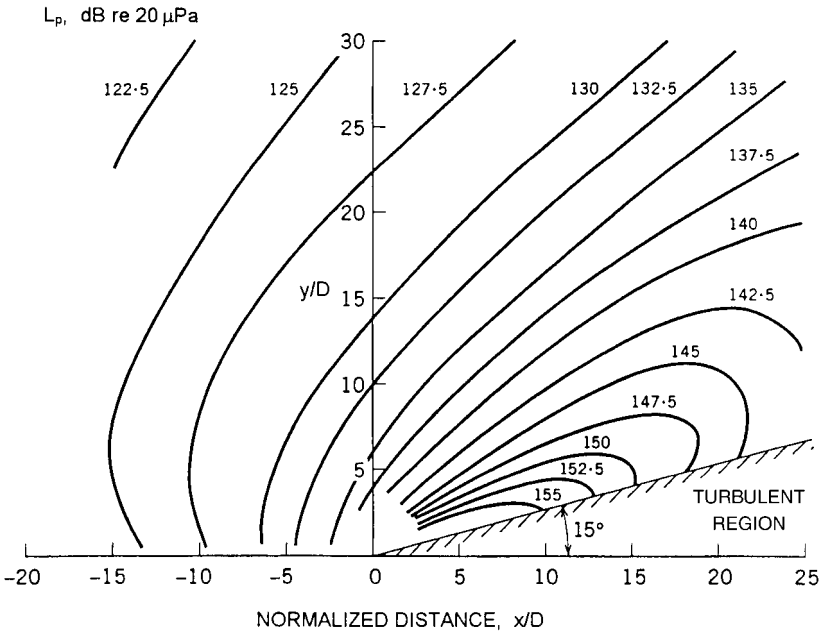


FIGURE 29.33 Jet noise near-field sound pressure levels. D = nozzle diameter, x = distance downstream of nozzle, y = distance from jet axis. (Reproduced with permission of ESDU International.⁷)

Jet noise spectra are broadband and peak at different frequencies for different locations in the near field.⁵⁻⁷ The spectra can be normalized in terms of a nondimensional frequency using jet nozzle diameter D and jet velocity V_j as the normalizing parameters. Then, the frequency of the spectral peak lies in the range $0.1 < fD/V < 1.0$, depending on location relative to the nozzle, as shown in Fig. 29.34.⁷

The spatial distribution of the pressure phase for a jet noise near field can be presented in terms of the band-limited (e.g., one-third-octave band) crosscorrelation function^{5,8,9} (see Chap. 11) or the normalized cross-spectral density function $\gamma_p(\xi, f)$ (see Chap. 22), since the two functions are equivalent. Typical measured values of $\gamma_p(\xi, f)$ for jet noise pressures close to a jet^{8,9} are shown in Fig. 29.35. Frequency f is normalized with respect to separation distance ξ and the trace wavespeed of the incident sound, in order to permit scaling from one situation to another. Trace wavespeed V_i is the wave speed of the incident sound when projected onto the surface of the excited structure. Thus, for sound waves of speed c incident at an angle θ to the normal to the surface, the trace wavespeed is $c/\sin \theta$. The value of V_i is often frequency dependent and, in the case of the data in Fig. 29.35, has values of $1.43c$, $1.25c$, and $1.0c$ for frequencies 400, 500, and 800 Hz, respectively. These values of the

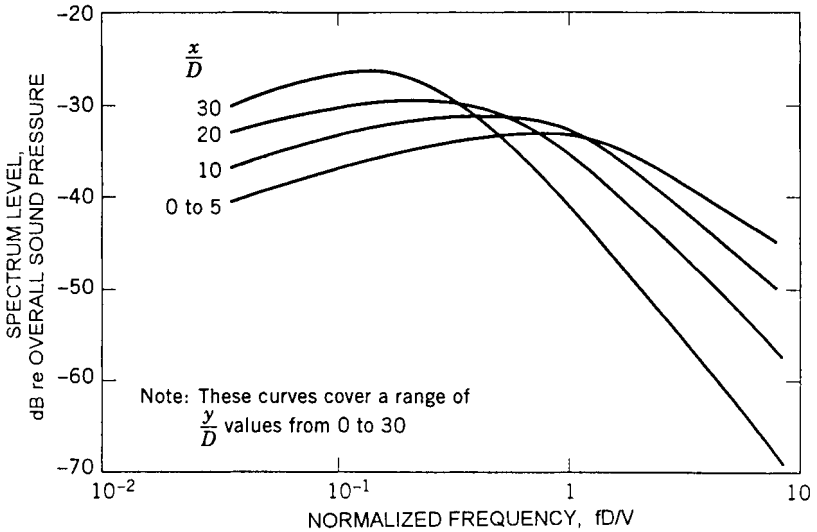


FIGURE 29.34 Normalized sound pressure spectra for several locations in jet noise near-field. V = jet velocity; D , x , y , as defined in Fig. 29.33. (Reproduced with permission of ESDU International.⁷)

trace wavelpeed correspond to angles of incidence of 44, 53, and 90°, respectively. The different angles of incidence are associated with the different locations in the jet exhaust of the effective noise sources for different frequencies. Figure 29.35 refers to measurements made in a plane passing through the jet axis. Corresponding information in a direction perpendicular to that plane are less well defined.

For convenient substitution into analytical models, the normalized cross-spectrum is often represented as an exponentially decaying cosine, with the general form

$$\gamma_p(\xi, f) = e^{-a k |\xi|} \cos(k \xi) \tag{29.59}$$

where a is a decay parameter and k is the wave number of the pressure field, where wave number is defined by

$$k = \frac{\omega}{V_t} = \frac{2\pi f}{V_t} \tag{29.60}$$

Curves of $\gamma_p(\xi, f)$ are shown in Fig. 29.35 for three values of the decay parameter a , namely, 0.05, 0.07, and 0.10.

Supersonic jet exhausts that are under- or overexpanded contain shockwaves that result in the generation of additional broadband noise and discrete frequency *screech*.¹ The screech consists of a fundamental component, whose frequency is a function of nozzle pressure ratio or flow Mach number, and several harmonics. The directivity of the screech noise is a function of harmonic order, with the fundamental having a maximum in the upstream direction and the second harmonic having a multilobed directivity pattern with peaks in directions perpendicular to the flow direction, as well as in the upstream direction.

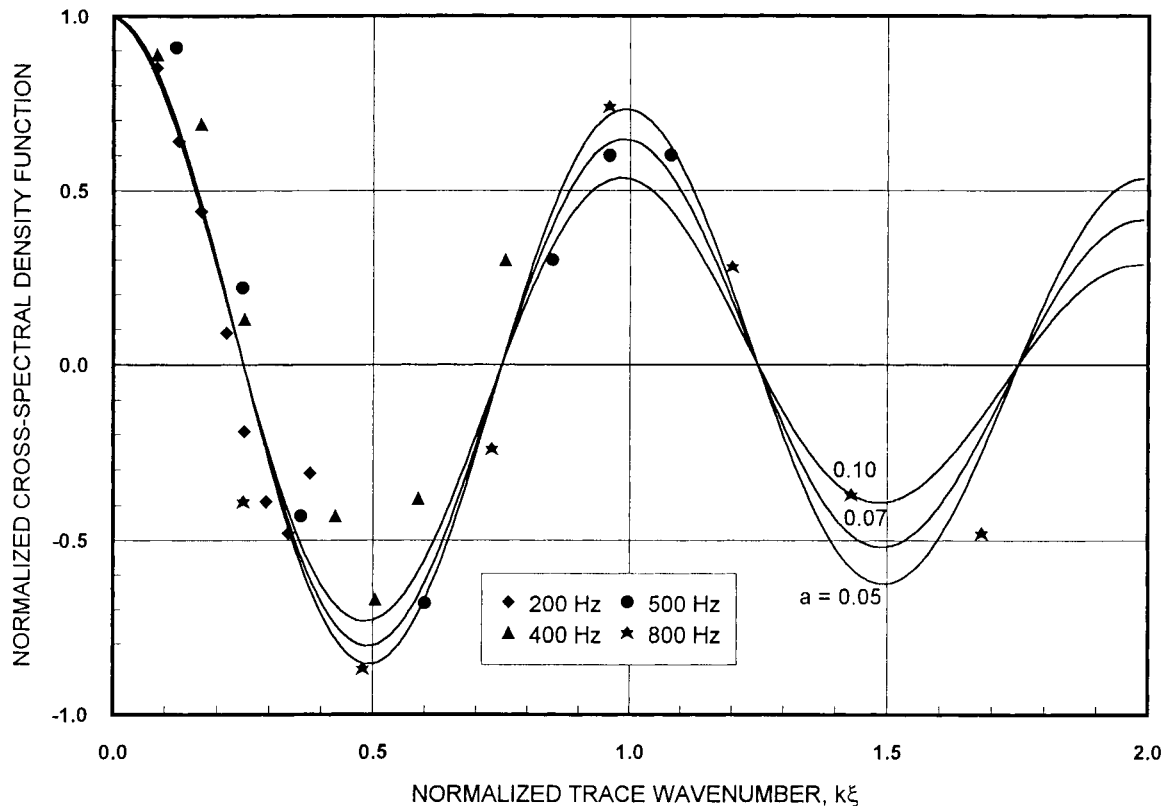


FIGURE 29.35 Example of normalized cross-spectral density function for jet noise near-field pressures. Test data collapsed with trace velocity $V_t = 1.43c$ (200, 400 Hz), $1.25c$ (500 Hz), and $1.0c$ (800 Hz). Continuous plots represent Eq. (29.59) with decay parameter $a = 0.05, 0.07$, and 0.10 . (Data from Richards and Mead.⁹)

ENGINE EXHAUST FLOWS

Powered lift aircraft utilize the exhaust from the engines to augment the lift generated by the wing and increase the effectiveness of the control surfaces, utilizing systems such as upper surface blowing and externally blown flaps.¹ By so doing, the surfaces of the aircraft are exposed to high sound pressure levels that are a combination of acoustic and aeroacoustic pressures. For example, sound pressure levels of up to 165 dB were measured on an airplane with upper surface blowing.¹⁰ In addition, the structure was heated to a temperature of 500 to 700°F (260 to 370°C). A similar situation exists on stealth aircraft where the engine exhaust flows over the upper surface of the aft structure so that the gases are cooled before they can be observed from below.¹⁰ Sound pressure levels greater than 180 dB are predicted in the neighborhood of the exhaust flows on hypersonic aircraft.¹⁰⁻¹²

PROPELLERS AND FANS

Propeller or fan noise consists of both broadband and discrete frequency components, but the pressure spectrum is dominated by discrete frequency components at the blade passage frequency of the propeller or fan and harmonics thereof. The blade passage frequency f_b is given by

$$f_b = \frac{\Omega B}{60} \quad (29.61)$$

where Ω is the rotational speed (rpm) of the propeller or fan and B is the number of blades. The spectra for counter-rotating propellers are more complex, with blade passage frequency components for each of the propellers plus interaction tones,¹³ as shown in Fig. 29.36. The spectrum in the figure also contains components for each individual blade of the propeller, because the blades are not identical.

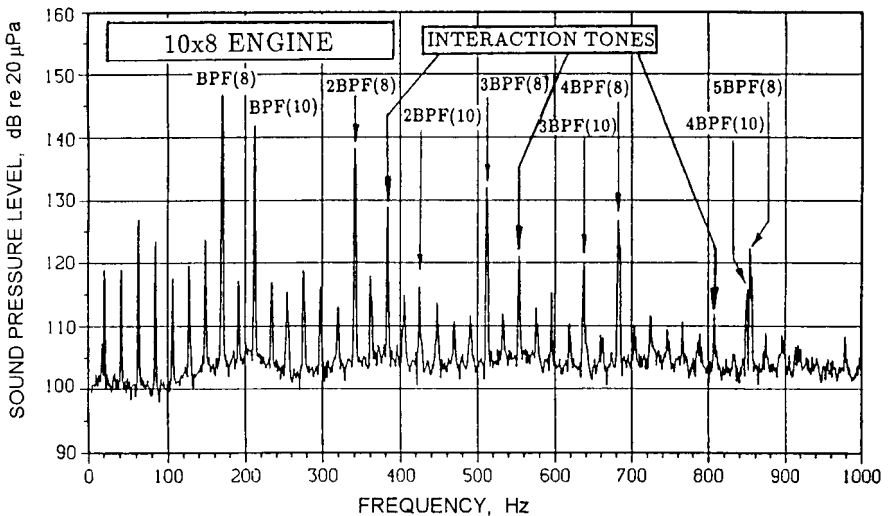


FIGURE 29.36 Spectrum for near-field sound pressure levels of high-speed, counter-rotating propeller with 8 and 10 blades. BPF(8) and BPF(10) denote blade passage frequencies for 8- and 10-blade propeller stages, respectively. (Simpson, Druez, Kimbrough, Brock, Burge, Mathur, Cannon, and Tran.¹³)

Sound pressure levels on the fuselage of multiengined general aviation aircraft are typically of the order of 130 dB at the blade passage frequency. High-speed propellers, with tip speeds that are supersonic under cruise conditions, have higher sound pressure levels on the order of 150 dB.¹³

Cross-spectrum measurements of propeller noise on a general aviation airplane¹⁴ show that the pressure field in the plane of rotation is an aerodynamic potential field that rotates with the propeller blades. Forward and aft of the plane of rotation the pressure field is acoustic and has the characteristics of propagating acoustic waves generated by sources located near the tips of the propeller blades. The spatial distribution of the cross-spectrum phase is more complicated for counter-rotating propellers.¹⁵

TURBULENT BOUNDARY LAYER

The dominant fluctuating pressures acting on launch vehicles, missiles, and aircraft in high-speed flight are associated with the turbulent boundary layer on the external surfaces of the vehicle. Similar fluctuating pressure fields are also encountered on other moving vehicles including automobiles, particularly around the windshield, and high-speed elevators. These pressure fields have many of the characteristics of an acoustic pressure field, but the convection velocity of the pressure fluctuations over the surface may be subsonic in contrast to an acoustic field where the trace velocity is always equal to, or greater than, the speed of sound in the fluid. There are also differences in the cross-spectra.

Measurements of turbulent boundary layer pressure fluctuations have been made in wind tunnels, on aircraft in flight, and underwater.^{9,16-18} The measurements have included both subsonic and supersonic flow conditions, but the emphasis has been on subsonic conditions. A combination of analytical and empirical methods has resulted in representations for the various characteristics of turbulent boundary layer pressure fields for both attached and separated flow.

For an attached turbulent boundary layer, taking into account compressibility effects, the rms pressure p_{rms} can be expressed as a function of Mach number, in relationships such as¹⁹

$$\frac{p_{\text{rms}}}{q} = \frac{0.006}{1 + 0.13M^2} \quad (29.62)$$

where q is the *dynamic pressure* of the flow, given by $q = \frac{1}{2}\rho V^2$ where V is velocity, ρ is the density of the fluid, and M is the flow Mach number, defined at some location such as free stream or the edge of the boundary layer. Corresponding relationships can be developed for separated flow conditions.

The pressure spectrum $G_p(\omega)$ for an attached turbulent boundary layer is broadband and can be represented by a relationship of the form¹⁹

$$\frac{G_p(\omega)V}{q^2\delta^*} = \frac{2\kappa(p_{\text{rms}}/q)^2}{\pi \left[1 + \left(\frac{\kappa\omega\delta^*}{V} \right)^2 \right]} \quad (29.63)$$

where κ is a function of flow Mach number, V is the flow velocity, and δ^* is the *boundary layer displacement thickness*. The boundary layer displacement thickness is the distance that the surface beneath the boundary layer would have to move outward and normal to itself to account for the differences in the rate of mass flow with the boundary layer present and, hypothetically, without the boundary layer. Separated turbulent boundary layers in the neighborhood of steps, ramps, and other sur-

face discontinuities have higher pressure levels at low frequencies than is the case for attached boundary layers, as shown in Fig. 29.37.¹⁸ Pressure spectrum and frequency are normalized in Fig. 29.37 with respect to *boundary layer thickness* δ rather than boundary layer displacement thickness δ^* . Boundary layer thickness can be defined as the distance from the surface at which the flow velocity reaches 99.5 percent of the free stream velocity. Equation (29.63) can be modified to take into account the low-frequency shifts seen in Fig. 29.63 by replacing κ with $C\kappa$, where $C > 1$. The presence of oscillating shockwaves further increases the low-frequency component of the pressure spectrum,¹⁸ as can be seen in Fig. 29.37.

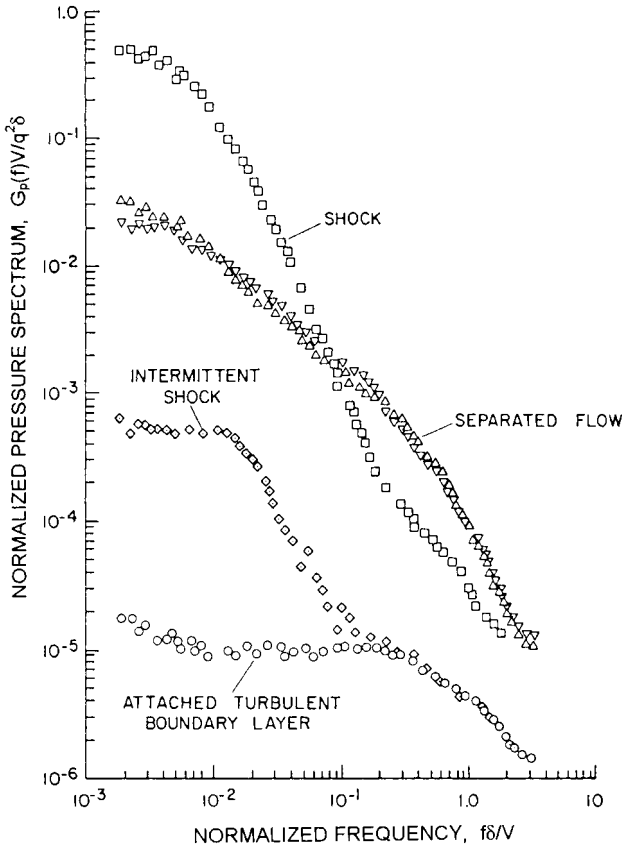


FIGURE 29.37 Pressure spectra beneath different turbulent boundary layers in supersonic flow. $G_p(f) = G_p(\omega)/2\pi$, V = flow velocity, q = flow dynamic pressure, δ = boundary layer thickness. (Coe, Chyu, and Dods.¹⁸)

Normalized cross-spectra or band-limited cross-correlation functions have been measured for attached turbulent boundary layers.^{16,17} The measured data indicate that the normalized cross-spectrum is dependent on the thickness of the boundary layer δ as well as on the convection speed V_c of the pressure field and the separation distance ξ between the measuring points. Empirical relationships such as²⁰

$$\gamma(\xi, \omega) = \exp \left\{ - \left[\left(\frac{0.1\omega}{V_c} \right)^2 + \left(\frac{0.27}{\delta} \right)^2 \right]^{0.5} |\xi| \right\} \cos \left(\frac{\omega \xi}{V_c} \right) \tag{29.64}$$

have been proposed for attached turbulent boundary layers. There is little corresponding information for separated boundary layers, where the flow is much more complicated.

IMPULSIVE SOUNDS

Impulsive sounds, such as sonic booms generated by airplanes in supersonic flight¹ and blast waves from explosions, can cause transient vibration of a structure.

ANALYTICAL METHODS

It is often assumed in the analysis of structural response to acoustic excitation that the structure responds in a linear manner, so that there is a linear relationship between excitation force and structural response. However, this assumption may not be valid when the acoustic excitation levels are high. In that case the response is non-linear.

LINEAR ANALYSIS

Several different methods can be used to calculate the linear response of a structure to acoustical excitation. They include classical normal mode analysis, statistical energy analysis, and finite element analysis. Each method has its own advantages and disadvantages.

Classical Normal Mode Analysis. In the classical modal formulation,⁹ the acceleration autospectrum $G_a(\underline{x}, \omega)$ for location x and angular frequency ω can be written as

$$G_a(\underline{x}, \omega) = \omega^4 A^2 G_p(\omega) \sum_r \sum_s \psi_r(\underline{x}) \psi_s(\underline{x}) H_r(\omega) H_s^*(\omega) j_{rs}^2(\omega) \tag{29.65}$$

where A is the area of the structure exposed to the excitation, $G_p(\omega)$ is the excitation pressure spectrum, $\psi_r(\underline{x})$ is the mode shape of mode of order r , $H_r(\omega)$ is the structural mode response function, $j_{rs}^2(\omega)$ is the cross acceptance that describes the spatial coupling between the excitation pressure field and the structural mode shapes, and an asterisk denotes a complex conjugate. The *cross acceptance* is defined by

$$j_{rs}^2(\omega) = \frac{1}{A^2 G_p(\omega)} \iint G_p(\underline{x}, \underline{x}', \omega) \psi_r(\underline{x}) \psi_s(\underline{x}') d\underline{x} d\underline{x}' \tag{29.66}$$

and the *structural mode response function* is defined by

$$|H_r(\omega)|^2 = M_r^{-2} [(\omega_r^2 - \omega^2)^2 + \eta_r^2 \omega_r^4]^{-1} \tag{29.67}$$

where η_r is the damping loss factor ($\eta_r = 2\zeta_r$, where ζ_r is the damping ratio), M_r is the modal mass, and ω_r is the resonance frequency of mode r . The *modal mass* is defined as

$$M_r = \int_A m \psi_r^2(\underline{x}) d\underline{x} \quad (29.68)$$

where m is the mass per unit area for a panel of area A . For a uniform panel with simply supported boundaries, $M_r = mA/4$. Prediction methods for ω_r can be found in Chap. 7.

If the damping is small and the fluid loading is negligible (which is usually true in air but not in water), the vibration is dominated by the response at the resonance frequencies and contributions from the cross terms ($r \neq s$) can be neglected. Then Eq. (29.65) becomes

$$G_a(\underline{x}, \omega) = \omega^4 A^2 G_p(\omega) \sum_r \psi_r^2(\underline{x}) |H_r(\omega)|^2 j_r^2(\omega) \quad (29.69)$$

In Eq. (29.69), the cross acceptance of Eq. (29.66) is replaced by the *joint acceptance*

$$j_r^2(\omega) = \frac{1}{A^2 G_p(\omega)} \iint G_p(\underline{x}, \underline{x}', \omega) \psi_r(\underline{x}) \psi_r(\underline{x}') d\underline{x} d\underline{x}' \quad (29.70)$$

Assuming that the structure has simply supported boundaries, and $G_p(\omega)$ and $j_r^2(\omega)$ vary slowly with ω in frequency band $\Delta\omega$, the space-average, mean square response in frequency band $\Delta\omega$ is

$$[a^2]_{\Delta\omega} \approx \frac{\omega^4 A^2}{4} G_p(\omega) \sum_r j_r^2(\omega) \int_{\Delta\omega} |H_r(\omega)|^2 d\omega \quad (29.71)$$

For small damping

$$\int_{\omega} |H_r(\omega)|^2 d\omega \approx \frac{\pi}{2\omega_r^3 \eta_r M_r^2} \quad (29.72)$$

and Eq. (29.71) reduces to

$$[a^2]_{\Delta\omega} \approx \frac{\omega^4 A^2 \pi}{8} G_p(\omega) \sum_{r \in \Delta\omega} \frac{j_r^2(\omega)}{\omega_r^3 M_r^2 \eta_r} \quad (29.73)$$

The notation $r \in \Delta\omega$ signifies that the summation is over all modes of order r whose resonance frequency ω_r lies in the frequency band $\Delta\omega$. From Eq. (29.73), the acceleration spectral density, averaged in space and frequency, is

$$\langle G_a(\omega) \rangle_{A, \Delta\omega} = \frac{[a^2]_{\Delta\omega}}{\Delta\omega} \approx \frac{\omega^4 A^2 \pi}{8 \Delta\omega} G_p(\omega) \sum_{r \in \Delta\omega} \frac{j_r^2(\omega)}{\omega_r^3 M_r^2 \eta_r} \quad (29.74)$$

where $\langle \rangle_{A, \Delta\omega}$ denotes averaging over area A and frequency band $\Delta\omega$. It can be seen in Eqs. (29.69), (29.73), and (29.74) that the two functions representing the excitation pressure field are the pressure autospectrum, $G_p(\omega)$, and the joint acceptance, $j_r^2(\omega)$.

The classical normal mode approach of Eq. (29.69) is an accurate way to predict structural response to acoustic or aeroacoustic pressure fields, provided that the relevant details of the structure and pressure field are known and represented correctly. However, that is often not the case. It is difficult to obtain the cross-spectrum data for the pressure field and approximations have to be made. Also, an accurate description of the normal modes and resonance frequencies of the structure is not always available, especially for complicated structures. Experimental procedures (see Chap. 21) and analytical methods, such as finite element analysis (see Chap. 28, Part II), might be used to obtain normal mode information, but both methods

become increasingly inaccurate as frequency increases. One solution is to resort to averaging techniques such as Eq. (29.73) or (29.74), but that has the disadvantage of eliminating some of the details in the results. Statistical energy analysis (see Chap. 11) is a further step in the averaging process.

Analysis of structural response to sound underwater is complicated by the fact that fluid loading is no longer negligible and has to be included in the analytical model.^{21,22} The effect of fluid loading depends on whether the frequency of interest is below or above the *critical frequency*, which is defined as the frequency at which the trace wavespeed of the sound field is equal to the wavespeed of the flexural or bending waves in the structure. At frequencies below the critical frequency, fluid loading essentially acts as an entrained mass that has to be included as a second mass term in the equations of motion.²² At frequencies above the critical frequency, the fluid loading influences the radiation resistance and the sound radiation into the fluid.²²

Joint Acceptance. The joint acceptance function describes the efficiency by which a particular pressure field can excite a structure. For a given pressure spectrum $G_p(\omega)$, different types of excitation, with different joint acceptance functions, will generate different vibration levels in the responding structure. For example, turbulent boundary layer pressure fluctuations will produce different vibration levels than will jet noise of the same pressure level.

Simplifying assumptions are usually introduced so that the joint acceptance can be obtained in closed form. Specifically, it is commonly assumed that the pressure field is homogeneous, so that \underline{x} and \underline{x}' can be replaced by $\underline{\xi}$, where $\underline{x}' - \underline{x} = \underline{\xi}$. The vector $\underline{\xi}$ has components ξ_x and ξ_y in the x and y directions, respectively. Also, it is assumed that the joint acceptance is separable in the x and y directions. Finally, it is assumed that the structure is simply supported at the boundaries. Then, the component of the joint acceptance in the x -direction is

$$f_m^2(\omega) = \frac{1}{A^2} \int_{L_x} \int \gamma_x(\xi_x, \omega) \cos(k_x \xi_x) \sin\left(\frac{m\pi x}{L_x}\right) \sin\left(\frac{m\pi x'}{L_x}\right) dx dx' \quad (29.75)$$

with

$$\gamma_x(\xi_x, \omega) = \frac{|G_p(\xi_x, 0, \omega)|}{G_p(\omega)} \quad (29.76)$$

and mode order $r \equiv (m, n)$. Similar relationships apply in the y -direction.

Closed-form joint acceptance functions for three different types of excitation, namely, attached turbulent boundary layer, jet noise, and diffuse (reverberant) sound field, are given in Ref. 20. Typical nondimensional joint acceptance curves based on Eqs. (29.75), (29.76), and (29.59) are shown in Fig. 29.38, for the case where the decay parameter a in Eq. (29.59) has a value of 0.1. The joint acceptance for the first mode shape ($n = 1$) has a maximum value at zero wave number or frequency, but the joint acceptance for each of the other modes has a maximum value at a nonzero value of frequency. Those maxima for the higher-order modes occur when the wave number of the excitation is equal to the flexural wave number for the structural mode, a condition known as *coincidence*.

Statistical Energy Analysis. Statistical energy analysis (SEA) makes the general assumption that it is not practical to represent all the details of a structure in a given response prediction procedure (see Chap. 11). Thus, ensemble averaging is per-

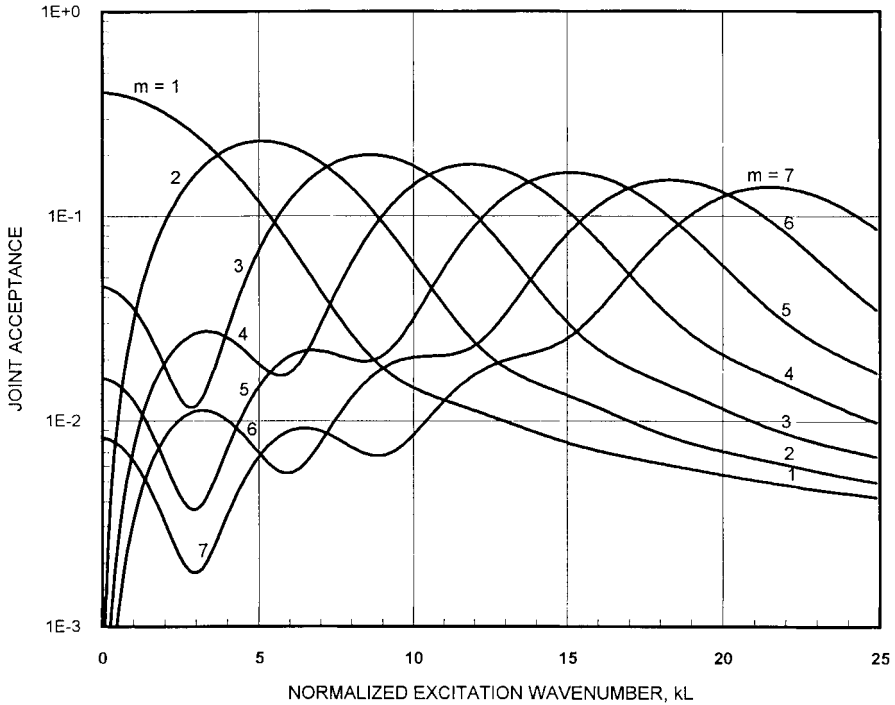


FIGURE 29.38 Joint acceptance curves based on Eqs. (29.75), (29.76), and (29.59), with decay parameter $a = 0.1$. L = length of panel, m = mode order, k = excitation wave number [Eq. (29.60)].

formed over a series of similar, but slightly different, structures to obtain an average response. In practice, ensemble averaging is time-consuming, so it is replaced by frequency averaging.

Equation (29.74) leads to a typical SEA relationship for simply supported panels, specifically,

$$\langle G_a(\omega) \rangle_{A, \Delta\omega} = G_p(\omega) \frac{2\pi\omega n_r(\omega)}{m^2} \frac{\langle j_r^2(\omega) \rangle_{\Delta\omega}}{\langle \eta_r \rangle_{\Delta\omega}} \tag{29.77}$$

where $\langle \rangle_{\Delta\omega}$ denotes averaging over frequency, $n_r(\omega)$ is the modal density of the structure, and m is the mass/unit area of the panel (assumed uniform). The frequency-band-averaged joint acceptance is

$$\langle j_r^2(\omega) \rangle_{\Delta\omega} = \frac{1}{N} \sum_{r=1}^N j_r^2(\omega) \tag{29.78}$$

where N is the number of modes with resonance frequencies in frequency band $\Delta\omega$. The modal density of the structure is defined by

$$n_r(\omega) = \frac{dN}{d\omega} \tag{29.79}$$

For a flat panel,

$$n(\omega) = \frac{\sqrt{3}A}{2\pi h c_L} \quad (29.80)$$

where h is the panel thickness and c_L is the *longitudinal wave speed* in the structure given by

$$c_L = \sqrt{\frac{E}{\rho(1-\nu^2)}} \quad (29.81)$$

In Eq. (29.81), E is Young's modulus of the structural material, ρ is the material density, and ν is Poisson's ratio.

The use of SEA techniques to simplify the analysis has the advantage that the response can be calculated to high frequencies with minimum computing time, but there is the disadvantage that the use of space- and frequency-averaging methods means that structural response cannot be predicted for a specific point on the structure nor at a specific frequency. Additional methods have to be used to supplement the SEA calculations. Further discussion on statistical energy analysis can be found in Chap. 11.

SEA is of limited value at low frequencies where modes are sparse ($N < 3$, say). The method can still be used but the variance of the results becomes large. However, classical normal mode and finite element methods are applicable at low frequencies. In practice, it is often found that there is a midfrequency range, above the usual frequency range for normal mode and finite element methods and below the usual frequency range for SEA, where none of the methods is very accurate.

Finite Element Analysis. In finite element analysis, a continuous structure is modeled as an array of grid points connected by appropriate elements (see Chap. 28, Part II). This means that the continuously distributed sound pressure field has to be represented as an array of discrete forces applied at the grid points. The forces have to be given autospectral functions that take into account the frequency characteristics and amplitudes of the excitation pressure field, and the structural area attributed to each grid point. In addition, the forces at each pair of grid points have to be assigned the appropriate cross-spectrum function based on the spatial separation between the grid points.

The response of the structure at location \underline{x} can be calculated using relationships of the form²³

$$G_a(\underline{x}, \omega) = \sum_{j=1}^q \sum_{k=1}^q H_{jx}^{*T}(\omega) \frac{A_x}{A_j} G_{jk}(\omega) \frac{A_x}{A_k} H_{kx}(\omega) \quad (29.82)$$

where $H_{jx}(\omega)$ is the frequency response function between the j th input and the response location \underline{x} , $G_{jk}(\omega)$ is the cross-spectrum between the j th and k th inputs, A_j is the area associated with the j th input, and A_x is the area associated with the response location. The frequency response function $H_{jx}^{*T}(\omega)$ is the transpose of the complex conjugate of $H_{jx}(\omega)$. Basic details of the finite element method can be found in Chap. 28, Part II.

Successful application of finite element analysis to the calculation of the response of a structure to acoustic or aeroacoustic pressure fields requires that there be an adequate number of degrees-of-freedom in the finite element model and an appropriate representation of the pressure field auto- and cross-spectra. In principle, finite element methods can be applied over the entire frequency range of interest, but that is not necessarily true in practice. As frequency and number of modes increases, it

becomes more difficult to provide an accurate description of the structure including boundary conditions. It also becomes more difficult to represent the details of the pressure field cross-spectrum. Finally, the time required to perform the necessary computations can become excessive. Thus, the finite element method suffers from the same disadvantages as does the classical normal mode method.

Damping. It is obvious from Eqs. (29.73) and (29.74) that damping is an important parameter in determining the magnitude of the structural response to acoustic or aeroacoustic excitation, since the mean square acceleration is inversely proportional to the damping loss factor η_r . The damping loss factor in Eq. (29.73) is composed of three components, as follows:

$$\eta_r = \eta_{r,\text{struc}} + \eta_{r,\text{rad}} + \eta_{r,\text{aero}} \quad (29.83)$$

The structural loss factor, $\eta_{r,\text{struc}}$, represents the damping due to material properties of the structure and mechanisms such as gas pumping at riveted joints and slip damping (see Chap. 36). It also represents damping due to any applied treatments (see Chap. 37). The radiation damping loss factor, $\eta_{r,\text{rad}}$, represents damping associated with the radiation of sound as a consequence of the vibration of the structure. This can be a significant contribution for structures such as composite structures that are very lightly damped. For structures in vacuo, $\eta_{r,\text{rad}} = 0$. The aerodynamic damping loss factor, $\eta_{r,\text{aero}}$, represents the damping associated with the presence of nonzero mean flow over the structure. Additional information on the damping of structures can be found in Refs. 24 and 25.

NONLINEAR VIBRATION

When excitation sound levels become too high, the response of a structure becomes nonlinear and linear analysis methods for the prediction of structural vibration are inaccurate. There are several situations where nonlinear response can be important. They include vibration where the displacement of the structure is no longer small with respect to the panel thickness, rattle induced by impulsive or low-frequency noise, and *snap-through* response of curved or buckled plates. Snap-through motion occurs when the local curvature of a panel that is curved by design or by buckling, jumps from one direction to another. Buckling can be caused, for example, by thermal stresses induced by high temperatures. Nonlinear response can be in the form of a hardening or softening spring (see Chap. 4), or instability conditions with snap-through motion.

Response characteristics often associated with nonlinear vibration are (1) the response amplitude no longer increasing in proportion to the amplitude of the excitation, (2) the resonance frequencies of the response modes changing with excitation amplitude, and (3) broadening of resonance peaks, which is attributed to nonlinear damping. The first two phenomena are demonstrated in Fig. 29.39, which shows the response of a panel to a sound field generated by a siren.²⁶ The response in the first mode, in terms of amplitude and resonance frequency, becomes nonlinear when the sound pressure reaches a level of about 102 dB.

Various approaches have been developed for the prediction of nonlinear response of a structure to acoustic excitation,²⁷⁻³¹ but they often have very limited application. Characteristics of nonlinear vibration and several approximate methods for analyzing the vibration are reviewed in Chap. 4. Nonlinear analytical methods that give closed-form quantitative results are usually limited to simple structures.

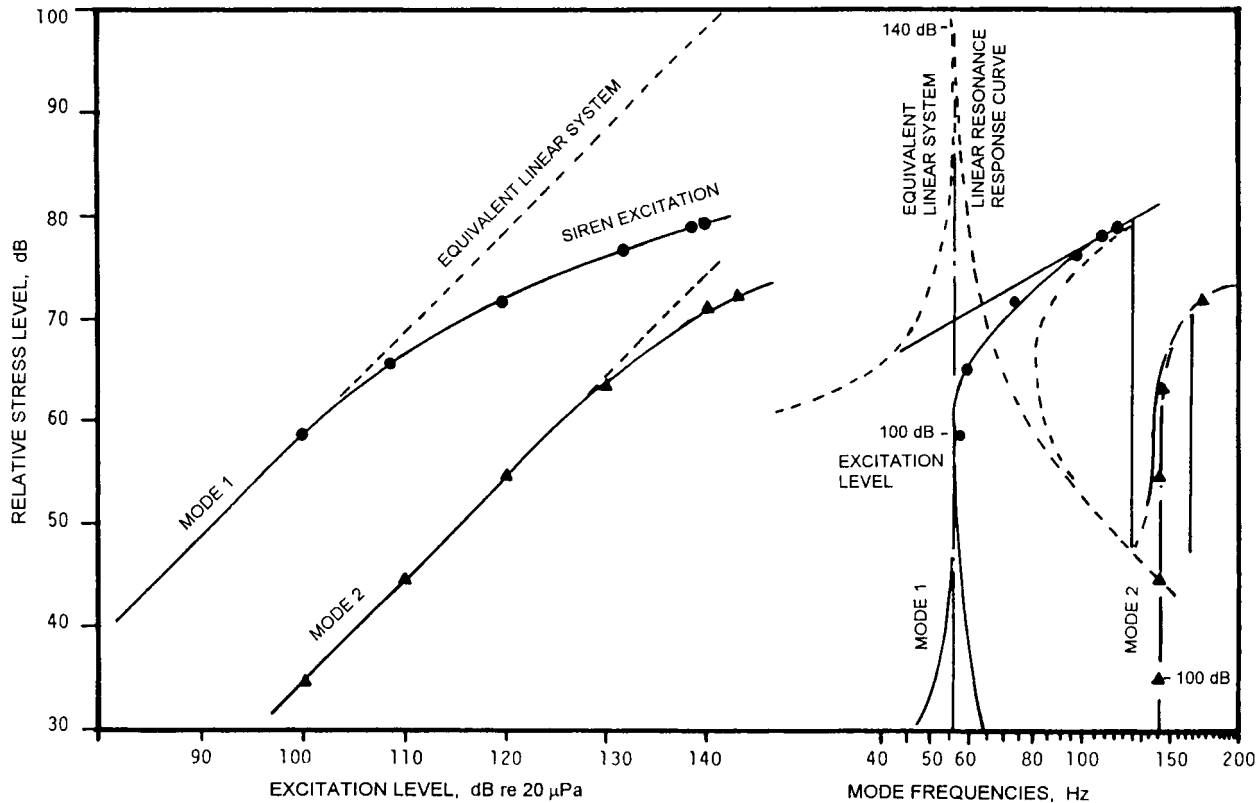


FIGURE 29.39 Nonlinear stress response characteristics for flat panel exposed to siren excitation. Panel with clamped edges, panel length = 12 in. (0.30 m). (Mei.²⁶)

Approximate methods are usually required for complex structures such as those found in aerospace applications. Other approaches include numerical methods, such as the Monte Carlo approach, and finite element methods using nonlinear element stiffness matrices. However, the methods are often restricted to simple acoustic pressure fields such as (1) plane waves at normal incidence, with the pressure uniform in both amplitude and phase over the entire surface of the structure; (2) plane acoustic waves at grazing incidence; or (3) uncorrelated pressure fields. Furthermore, structural response is often limited to a single mode.

The Monte Carlo method³¹ is based on the numerical generation of a large number of random, sample excitations and the calculation of the response to each sample. The method can be used for both linear and nonlinear responses to random excitations, and it could be a feasible approach for nonlinear vibration where closed-form or approximate solutions are not possible, although the method requires the use of high-speed digital computers. One example of a second-order, nonlinear equation of motion for a panel is

$$dX_{ij}/dt^2 + 2\zeta_{ij}\omega_{ij}(dX_{ij}/dt) + \omega_{ij}^2 X_{ij} + N(X_{ij}, dX_{ij}/dt) = F_{ij}(t) \quad (29.84)$$

where X_{ij} are the components of generalized coordinates, ω_{ij} are the natural frequencies of a linear system, ζ_{ij} are the modal damping coefficients, N is the nonlinear system operator, and $F_{ij}(t)$ are the generalized random forces.

The time-domain Monte Carlo method consists of three basic steps:³¹ (1) random inputs for $F_{ij}(t)$ are generated using simulation procedures of random processes; (2) the equations of motion, such as Eq. (29.84), are solved numerically for each random value of $F_{ij}(t)$; and (3) statistical moments and other needed quantities of the random response $X_{ij}(t)$ are computed for ensemble averages. If the system is ergodic (see Chap. 1), the ensemble averaging can be replaced by time averaging, with a saving in computing time.

In many aerospace situations, the structure is exposed to high temperatures and the structural vibration is strongly dependent on thermal stresses induced by a thermal environment. The effect is taken into account in some procedures by applying the acoustic and thermal loads in sequence. A more appropriate analysis of nonlinear response of aerospace structures considers acoustic and thermal loads simultaneously.²⁷

Structural damping is often represented as linear damping. However, nonlinear damping can be represented, for example, by replacing linear damping in Duffing's equation (see Chap. 4) with a nonlinear damping term³² such as $\omega_0\eta(1 + \alpha q^2)dq/dt$.

ACOUSTIC FATIGUE

Acoustically induced structural vibration results in oscillating stresses. The stress levels may be low but, because of the frequencies involved, typically 100 to 500 Hz, the number of stress reversals can be large enough at stress concentration points to create fatigue cracks. This phenomenon is called high-cycle fatigue, acoustic fatigue, or sonic fatigue.³³ Most examples of failures induced by sonic fatigue occur in aircraft structures in the form of skin failures along rivet lines, skin debonding in sandwich panels, and failure in internal attachment structures.^{5,6}

In many cases the stresses induced by acoustic pressure fields are dominated by response in the first mode of vibration of a panel, and the acoustical wavelength is large relative to the dimensions on the panel. Then, the sound pressures are essen-

tially in phase over the panel, and details of the pressure correlation are of minor importance. The mean square stress $\sigma^2(t)$ can be estimated using the approximation⁶

$$\sigma^2(t) \approx K \frac{\pi}{4\eta} f_n G_p(f_n) \left(\frac{\sigma_o}{F_o} \right)^2 \quad (29.85)$$

where f_n is the frequency of the dominant mode of order n , $G_p(f_n)$ is the spectral density of the excitation pressure at frequency f_n , η is the damping ratio, and σ_o is the stress at the point of interest due to a uniform static pressure of magnitude F_o . Equation (29.85) is based on early work³⁴ for a single degree-of-freedom system. The factor K is included in Eq. (29.85) so that the equations can be modified to fit particular structural configurations and materials. There are cases where acoustic fatigue is caused by vibration of several modes, not just one. Thus, alternative prediction procedures are required that extend the approach in Eq. (29.85) to higher-order modes and complex shapes, and estimate the influence of acoustical wavelength.¹²

It is apparent from Eq. (29.85) that increasing the damping of a structure would decrease the stresses. Thus, the application of damping material will reduce the likelihood of acoustic fatigue. For example, damping treatment was applied to the fuselage structure of a test airplane with high-speed propellers to minimize the likelihood of acoustic fatigue in the plane of rotation of the propellers.¹³ Applied damping techniques are described in Chap. 37 and the wider aspects of passive vibration control are discussed in Ref. 35.

LABORATORY TESTING OF STRUCTURES AND EQUIPMENT

Laboratory tests are often required to supplement or validate analysis, evaluate new structural designs, or develop a database of fatigue life for different environmental conditions or for new materials, especially composites. Acoustical environments of aircraft and space vehicles can reach overall sound pressure levels in the range 170–180 dB in local areas. Consequently, there is a need to develop similar levels in the laboratory with the appropriate frequency distributions. Two test environments, the progressive wave tube and the reverberant chamber, are used for many of the laboratory tests. The purposes of the testing are to find weak points in the structural design or in the manufacturing process, or to determine whether or not the structure will have a satisfactory fatigue life (see Chap. 20). The progressive wave tube and reverberant chamber play different roles in this process.

PROGRESSIVE WAVE TUBES

A *progressive wave tube* consists of duct with a sound source at one end and a sound-absorbing termination at the other end. It is used to expose structural components, such as a panel, to high-intensity sound pressure levels for long periods of time so as to evaluate the susceptibility of the structure to acoustic fatigue. The test structure is mounted in one wall of the tube and exposed to sound waves traveling along the tube at grazing incidence.^{5,9,10,36} Relatively small test specimens are used because of the difficulty of generating, in the laboratory, very high sound pressure levels over large areas.

Due to concerns about the effect of high temperatures for some applications,

such as aircraft-powered lift devices, the structure beneath the engine exhaust of stealth aircraft, and the vehicle structure of hypersonic vehicles, facilities have been constructed that permit the heating of the test specimen at the same time that it is being exposed to the high-intensity sound pressure levels. The acoustic excitation is limited to the lower frequencies because of constraints on the source, which usually consists of several electropneumatic modulators with broadband random acoustical outputs. However, the lower frequencies are usually responsible for the highest stresses that determine acoustical fatigue life.

A typical progressive wave tube is shown in Fig. 29.40. The number of electro-pneumatic modulators is determined by the size of the duct, and the desired maximum sound pressure levels and frequency range. The number of modulators can range from 2 to 12, generating maximum sound pressure levels from 170 to over 180 dB with frequency ranges varying from 30–500 Hz to 50–1500 Hz.^{9,10,36} Test panel sizes range from 1 to 20 ft² (0.1 to 2 m²).

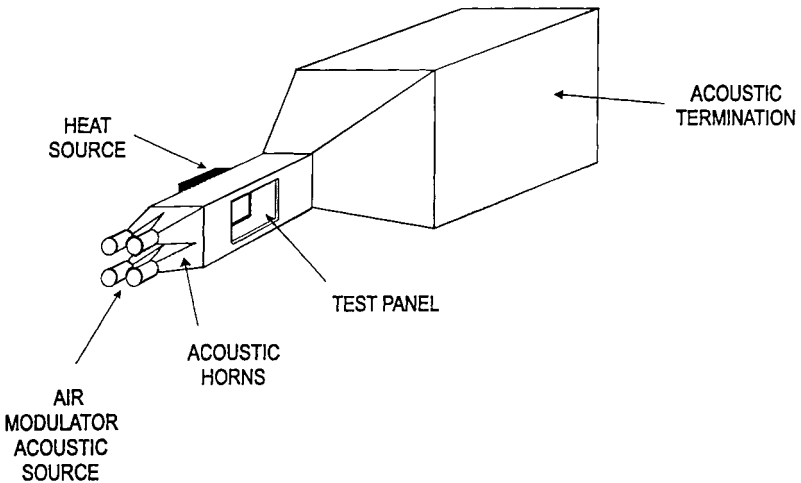


FIGURE 29.40 Typical progressive wave tube. (Shimovetz and Wentz.¹⁰)

REVERBERATION CHAMBERS

Reverberation chambers can be used to expose large structures to sound pressure levels typical of those encountered in service. A reverberation chamber is an enclosure with thick, rigid walls and smooth interior surfaces that strongly reflect sound waves.³⁷ Acoustic noise is introduced into the chamber at one or more locations, usually with air modulators mounted in one or more of the walls. Assuming that the acoustic noise source is random in character, it produces a sound field within the chamber that becomes increasingly homogeneous (a uniform sound pressure level throughout the chamber) as the wavelength of the sound becomes small relative to the minimum dimension of the chamber. Further, the sound field inside the chamber approaches a diffuse noise field, where *diffuse noise* is defined as a sound field where the sound waves at any point arrive from all directions with equal intensity and random phase. High-intensity reverberation chambers typically have an interior volume

of 7000 to 350,000 ft³ (200 to 10,000 m³), and are capable of producing sound pressure levels in an empty chamber of 150 to 160 dB over a frequency range from 0.1 to 10 kHz.³⁸

The vibration response of a test item to the acoustic excitation in a reverberation chamber can be measured by suspending the test item near the middle of the chamber, applying acoustic excitation with the desired level and spectrum, and measuring the vibration response of the test item at all locations of interest. However, it must be remembered that the spatial cross-spectrum for the field in a reverberation chamber may be quite different from that for the sound field in the actual service environment of the test item. Specifically, as mentioned earlier, the sound field in a reverberation chamber with a random acoustic source will closely approximate a diffuse noise field, which has a normalized spatial cross-spectrum between any two points given by¹⁴

$$\gamma(\xi, \omega) = \frac{\sin(k\xi)}{k\xi} \quad (29.86)$$

where k is the wave number of the pressure field defined in Eq. (29.60), and ξ is the separation distance. It should be noted that this is quite different from the normalized cross-spectrum for the sound field produced by jet noise or a turbulent boundary layer, as given by Eqs. (29.59) and (29.64), respectively. Hence, the cross-acceptance function defined in Eq. (29.66), which couples the sound field to the test item, may be different. It follows that the vibration response of the test item may be different from that which occurs in the service environment.

The maximum sound pressure levels achievable in a reverberation chamber are not as high as those in a progressive wave tube, but reverberant chambers can accommodate larger structures. Thus, the two environments are usually used for different types of tests.

REFERENCES

1. Hubbard, H. H. (ed.): "Aeroacoustics of Flight Vehicles: Theory and Practice," Acoustical Society of America, Woodbury, N.Y., 1994.
2. Ungar, E. E., J. F. Wilby, and D. B. Bliss: "A Guide for Estimation of Aeroacoustic Loads on Flight Vehicle Surfaces," *AFFDL-TR-76-91*, February 1977.
3. Eldred, K. M.: "Acoustic Loads Generated by the Propulsion System," *NASA SP-8072*, June 1971.
4. McInerny, S. A.: *Noise Control Engineering Journal*, **38:5** (1992).
5. Hubbard, H. H., and J. C. Houbolt: "Vibration Induced by Acoustic Waves," chap. 48, in C. M. Harris and C. E. Crede (eds.), "Shock and Vibration Handbook," 1st ed., McGraw-Hill Book Company, Inc., New York, 1961.
6. Clarkson, B. L.: "Effects of High Intensity Sound on Structures," chap. 70, in M. J. Crocker (ed.), "Encyclopedia of Acoustics," John Wiley & Sons, Inc., New York, 1997.
7. Anon., "ESDU Engineering Data: Acoustic Fatigue Series," Vols. 1-7, ESDU International, London, 2000.
8. Trapp, W. J., and D. M. Forney, Jr. (eds.): "Acoustical Fatigue in Aerospace Structures," Syracuse University Press, Syracuse, N.Y., 1965.
9. Richards, E. J., and D. J. Mead (eds.): "Noise and Acoustic Fatigue in Aeronautics," John Wiley & Sons, Ltd., London, England, 1968.
10. Shimovetz, R. M., and K. R. Wentz: *AIAA Paper CEAS/AIAA-95-142* (1995).

11. Blevins, R. D., I. Holehouse, and K. R. Wentz: *Journal of Aircraft*, **30**:971 (1993).
12. Blevins, R. D.: *Journal of Sound and Vibration*, **129**:51 (1989).
13. Simpson, M. A., P. M. Druez, A. J. Kimbrough, M. P. Brock, P. L. Burge, G. P. Mathur, M. R. Cannon, and B. N. Tran: "UHB Demonstrator Interior Noise Control Flight Tests and Analysis," *NASA Contractor Report 181897*, October 1989.
14. Bendat, J. S., and A. G. Piersol: "Engineering Applications of Correlation and Spectral Analysis," 2d ed., John Wiley & Sons, Inc., New York, 1993.
15. Landmann, A. E., H. F. Tillema, and S. E. Marshall: "Evaluation of Analysis Techniques for Low-Frequency Interior Noise and Vibration of Commercial Aircraft," *NASA Contractor Report 181851*, October 1989.
16. Bull, M. K.: *Journal of Fluid Mechanics*, **28**:719 (1967).
17. Blake, W. K.: "Mechanics of Flow-Induced Sound and Vibration," Academic Press, Inc., Orlando, Fla., 1986.
18. Coe, C. F., W. J. Chyu, and J. B. Dods, Jr.: *AIAA Paper 73-996* (1973).
19. Laganelli, A. L., and H. F. Wolfe: *Journal of Aircraft*, **30**:962 (1993).
20. Cockburn, J. A., and A. C. Jolly: "Structural-Acoustic Response, Noise Transmission Losses and Interior Noise Levels of an Aircraft Fuselage Excited by Random Pressure Fields," *AFFDL-TR-68-2*, August 1968.
21. Fahy, F. J.: "Sound and Structural Vibration," Academic Press, London, England, 1985.
22. Ross, D.: "Mechanics of Underwater Noise," Peninsula Publishing, Los Altos, Calif., 1987.
23. Hipol, P. J., and A. G. Piersol: *SAE Paper 871740* (1987).
24. Soovere, J., and M. L. Drake: "Aerospace Structures Technology Damping Design Guide," *AFWAL-TR-84-3089*, December 1985.
25. Ungar, E. E.: "Vibration Isolation and Damping," chap. 71, in M. J. Crocker (ed.), "Encyclopedia of Acoustics," John Wiley & Sons, Inc., New York, 1997.
26. Mei, C.: "Large Amplitude Response of Complex Structures due to High Intensity Noise," *AFFDL-TR-79-3028*, April 1979.
27. Mei, C., and R. R. Chen: "Finite Element Nonlinear Random Response of Composite Panels of Arbitrary Shape to Acoustic and Thermal Loads," *WL-TR-1997-3085*, October 1997.
28. Mei, C., and C. K. Chiang: *AIAA Paper AIAA-87-2713* (1987).
29. Wolfe, H. F., C. A. Shroyer, D. L. Brown, and L. W. Simmons: "An Experimental Investigation of Nonlinear Behaviour of Beams and Plates Excited to High Levels of Dynamic Response," *WL-TR-96-3057*, October 1995.
30. Ng, C. F.: *Journal of Aircraft*, **26**:281 (1989).
31. Vaicaitis, R.: *Journal of Aircraft*, **31**:10 (1994).
32. Prasad, C. B., and C. Mei: *AIAA Paper AIAA-87-2712* (1987).
33. Clarkson, B. L.: "Review of Sonic Fatigue Technology," *NASA Contractor Report 4587*, April 1994.
34. Miles, J. W.: *Journal of Aeronautical Sciences*, **21**:753 (1954).
35. Mead, D. J.: "Passive Vibration Control," John Wiley & Sons, Ltd., Chichester, England, 2000.
36. Leatherwood, J. D., S. A. Clevenson, C. A. Powell, and E. F. Daniels: *Journal of Aircraft*, **29**:1130 (1992).
37. Hodgson, M., and A. C. C. Warnock: "Noise in Rooms," chap. 7, in L. L. Beranek and I. L. Ver (eds.), "Noise and Vibration Control Engineering," John Wiley & Sons, Inc., New York, 1992.
38. Lee, Y. A., and A. L. Lee: "High Intensity Acoustic Tests," *IES-RP-DTE040.1*, Institute of Environmental Sciences and Technology, Mount Prospect, Ill., 2000.